

MultiView Diffusion Maps

Ofir Lindenbaum¹ Arie Yeredor¹ Moshe Salhov² Amir Averbuch²

¹School of Electrical Engineering, Tel Aviv University, Israel

²School of Computer Science, Tel Aviv University, Israel

15-August-2015

Abstract

In this study we consider learning a reduced dimensionality representation from datasets obtained under multiple views. Such multiple views of datasets can be obtained, for example, when the same underlying process is observed using several different modalities, or measured with different instrumentation. Our goal is to effectively exploit the availability of such multiple views for various purposes, such as non-linear embedding, manifold learning, spectral clustering, anomaly detection and non-linear system identification. Our proposed method exploits the intrinsic relation within each view, as well as the mutual relations between views. We do this by defining a cross-view model, in which an implied Random Walk process between objects is restrained to hop between the different views. Our method is robust to scaling of each dataset, and is insensitive to small structural changes in the data. Within this framework, we define new diffusion distances and analyze the spectra of the implied kernels. We demonstrate the applicability of the proposed approach on both artificial and real data sets.

I. INTRODUCTION

High dimensional big datasets exist in various fields and it is difficult to analyze them as is. Extracted features are useful in analyzing these datasets. However, this approach requires some prior knowledge or model in order to identify the essential features. On the other hand, dimensionality reduction methods are purely unsupervised aiming to find a low dimensional representation that is based on the *intrinsic geometry* of the analyzed dataset that includes the connectivities among multidimensional data points within the dataset. A dimensionality reduction methodology reduces the complexity of processing a dataset while preserving the coherency of the original data such that clustering, classification, manifold learning and many other data analysis tasks can be applied effectively in the reduced space. Many methods such as Principal Component Analysis (PCA)[1], Multidimensional Scaling (MDS)[2], Local Linear Embedding [3], Laplacian Eigenmaps [4], Diffusion Maps (DM)[5] and more have been proposed to achieve dimensionality reduction. Exploiting the low dimensional representation yields various applications such as face recognition based on Laplacian Eigenmaps [4], Non-linear independent component analysis with DM [6], Musical Key extraction using DM [7] and many more. The DM framework extends and enhances ideas from other methods by utilizing a stochastic Markov matrix that is based on the local affinities between multidimensional data points to identify a lower dimension representation for the dataset. All the mentioned methods do not consider the possibility of having more than one view to represent the same process. An additional view can provide meaningful insight regarding the dynamical process that has generated and governed the data.

In this paper, we consider learning from data that is analyzed by multiple views. Our goal is to effectively utilize multiple views such as non-linear embedding, multi-view manifold learning, spectral clustering, anomaly detection and non linear system identification to achieve better analysis of high dimensional big data. Most dimensionality reduction methods suggest to concatenate the datasets into a single vector space. However, this methodology is sensitive to scalings of each dataset. It does not utilize for example the fact that noise in both datasets could be uncorrelated. It assumes that both datasets lie in one high dimensional space.

The problem of learning from two views has been studied in the field of spectral clustering. Most of these studies have focused on classification and clustering based on the spectral characteristics of the dataset while using two or more sampled views. Some approaches, which addressed this problem, are Bilinear Model [8], Partial Least Squares [9] and Canonical Correlation Analysis [10]. These methods are powerful for learning the relation between different views but do not provide insights separately or together into the low dimensional geometry or structure of each view. Recently, a few kernel based methods (e.g [11]) propose a model of co-regularizing kernels in both views in a way that resembles joint diagonalization. It is done by searching for an orthogonal transformation which maximizes the diagonal terms of the kernel matrices obtained from all views. A penalty term, which incorporates the disagreement between clusters among the views, was added. Their algorithm is based on alternating maximization procedure. A mixture of Markov chains is proposed in [12] to model the multiple views in order to apply spectral clustering. It deals with two cases in graph theory: directed and undirected graph where the second case is related to our work. This approach converges for the undirected graph problem to an average of Markov chains where each is constructed separately within the views. A way to incorporate given multiple metrics for the same data using a cross diffusion process is presented in [13]. However, the applicability of the suggested approach is limited only for a clustering

task. An iterative algorithm for spectral clustering is proposed in [14]. The idea is to iteratively modify each view using the representation of the other view. The problem of two manifolds, which are derived from the same dataset (i.e two views), is described in [15]. This approach is similar to Canonical Correlation Analysis [16] that seeks a linear transformation which maximizes the correlation among the views. It demonstrates the power of this method in canceling uncorrelated noise present in both views. Furthermore, [15] applies its method to a nonlinear system identification task. A similar approach is proposed in [17]. It suggests data modeling that uses a bipartite graph and then, based on the ‘minimum-disagreement’ algorithm, partitions the dataset. This approach attempts to minimize the cluster’s disagreement between multiple views.

In this work, we present a framework based on the construction in [17] and show that the approach is a special case of a more general diffusion based process. We build and analyze a new framework that generalizes the random walk model while using multiple views. Our proposed method utilizes the intrinsic relation within each view, as well as the mutual relations between views. The multiview is achieved by defining a cross diffusion process in which a specially structured Random Walk is imposed between the various views. The multiview method is robust to scalings of each view and it is insensitive to small structural changes in the dataset. Within this framework, we define new diffusion distances to analyze the spectra of the new kernels and compute the infinitesimal generator to where our kernel converges to. We explore the advantages of the proposed method for manifold learning and spectral clustering. It allows us to define a new semi-supervised learning method by sampling one view from a physical system and generating a second view using some prior which estimates the underlying physical model.

The paper has the following structure: Background is given in section II. Section III presents and analyzes the proposed framework, section V presents the experimental results following the conclusions in section VI.

II. BACKGROUND

A. General dimensionality reduction framework

Consider a high dimensional dataset $\mathbf{X} = \{\mathbf{x}_1, \mathbf{x}_2, \mathbf{x}_3, \dots, \mathbf{x}_M\} \in \mathbb{R}^{M \times N}$,. The goal is to find a low dimensional representation $\mathbf{Z} = \{\mathbf{z}_1, \mathbf{z}_2, \mathbf{z}_3, \dots, \mathbf{z}_M\} \in \mathbb{R}^{M \times S}$ such that $S \ll N$ and the local connectivities among the multidimensional data points are preserved. This problem setup is based on the assumption that the data is represented by a single vector space (single view).

B. Diffusion Maps (DM)

DM [5] is a dimensionality reduction method that finds the intrinsic geometry of the data. This framework is highly effective when the data is densely sampled from some low dimensional manifold that is not restricted to a linear manifold. Given a high dimensional dataset \mathbf{X} , the DM framework contains the following steps:

- 1) A kernel function $\mathcal{K} : \mathbf{X} \times \mathbf{X} \rightarrow \mathbb{R}$ is chosen. It is represented by a matrix $\mathbf{K} \in \mathbb{R}^{M \times M}$ which satisfies for all $(\mathbf{x}_i, \mathbf{x}_j) \in \mathbf{X}$ the following properties: Symmetry: $K_{i,j} = \mathcal{K}(\mathbf{x}_i, \mathbf{x}_j) = \mathcal{K}(\mathbf{x}_j, \mathbf{x}_i)$, positive semi-definiteness: $\mathbf{v}_i^T \mathbf{K} \mathbf{v}_i \geq 0$ for all $\mathbf{v}_i \in \mathbb{R}^M$ and $\mathcal{K}(\mathbf{x}_i, \mathbf{x}_j) \geq 0$. These properties guarantee that the matrix \mathbf{K} has real eigenvectors and non negative real eigenvalues of the matrix \mathbf{K} . A common example for such kernel is a Gaussian $K_{i,j} = \exp\{-\frac{\|\mathbf{x}_i - \mathbf{x}_j\|^2}{2\sigma_x^2}\}$ with an L_2 norm as the affinity measure between two data vectors;
- 2) By normalizing the kernel using \mathbf{D} where $D_{i,i} = \sum_j K_{i,j}$, we compute the following matrix elements:

$$P_{i,j} = \mathcal{P}(\mathbf{x}_i, \mathbf{x}_j) = [\mathbf{D}^{-1} \mathbf{K}]_{i,j}. \quad (1)$$

The resulting matrix $\mathbf{P} \in \mathbb{R}^{M \times M}$ can be viewed as the transition kernel of a (fictitious) Markov chain on \mathbf{X} , such that the expression $[\mathbf{P}^t]_{i,j} = p_t(\mathbf{x}_i, \mathbf{x}_j)$ describes the transition probability from point \mathbf{x}_i to point \mathbf{x}_j in t steps.

- 3) Spectral decomposition is applied to the matrix \mathbf{P} or to one of its powers \mathbf{P}^t to obtain a sequence of eigenvalues $\{\lambda_m\}$ and normalized eigenvectors $\{\psi_m\}$ that satisfies $\mathbf{P}\psi_m = \lambda_m\psi_m, m = 0, \dots, M-1$;
- 4) Define a new representation for the dataset \mathbf{X}

$$\Psi_t(\mathbf{x}_i) : \mathbf{x}_i \mapsto [\lambda_1^t \psi_1(i), \lambda_2^t \psi_2(i), \lambda_3^t \psi_3(i), \dots, \lambda_{M-1}^t \psi_{M-1}(i)]^T \in \mathbb{R}^{M-1}, \quad (2)$$

where t is the selected number of steps and $\psi_m(i)$ denotes the i^{th} element of ψ_m .

The main idea behind this representation is that the Euclidian distance between two data points in the new representation is equal to the weighted L_2 distance between the conditional probabilities $p_t(\mathbf{x}_i, :)$, and $p_t(\mathbf{x}_j, :)$, $i, j = 1, \dots, M$ (the i -th and j -th rows of \mathbf{P}^t). The following is referred as the Diffusion Distance

$$\mathcal{D}_t^2(\mathbf{x}_i, \mathbf{x}_j) = \|\Psi_t(\mathbf{x}_i) - \Psi_t(\mathbf{x}_j)\|^2 = \sum_{m \geq 1} \lambda_m^{2t} (\psi_m(i) - \psi_m(j))^2 = \|p_t(\mathbf{x}_i, :) - p_t(\mathbf{x}_j, :)\|_{\mathbf{W}^{-1}}^2, \quad (3)$$

where \mathbf{W} is a diagonal matrix with elements $W_{i,i} = \phi_0(i) = \frac{D_{i,i}}{\sum_{i=1}^M D_{i,i}}$. This equality was proven in [5].

- 5) The desired accuracy $\delta \geq 0$ is chosen for the diffusion distance defined by Eq. 3 such that $s(\delta, t) = \max\{\ell \in \mathbb{N} \text{ such that } |\lambda_\ell|^t > \delta |\lambda_1|^t\}$. By using δ , a new mapping of $s(\delta, t)$ dimensions is defined as $\Psi_t^{(\delta)} : X \rightarrow [\lambda_1^t \psi_1(i), \lambda_2^t \psi_2(i), \lambda_3^t \psi_3(i), \dots, \lambda_s^t \psi_s(i)]^T \in \mathbb{R}^{s(\delta, t)}$.

This approach was found useful in various fields but as previously noted it is limited to a single view representation. A common extension of this approach to multiple views is to concatenate the data from all views into one single vector space and then apply to it the diffusion framework. This approach assumes orthogonality of the sampled dimension which is an unrealistic assumption in many cases. Furthermore, this approach can create redundancy in some dimensions and requires scaling of each dimension separately such that none is preferable over the others. Previous studies such as [18], [19] have applied the DM framework to each view separately and then incorporated the learned mapping from various views. However they do not exploit the mutual relations which might exist between the various views in order to create the correct mapping.

III. MULTIVIEW DIMENSIONALITY REDUCTION

Problem Formulation: Given two sets of observations $\mathbf{X} = \{\mathbf{x}_1, \mathbf{x}_2, \mathbf{x}_3, \dots, \mathbf{x}_M\} \in \mathbb{R}^{D_1}$ and $\mathbf{Y} = \{\mathbf{y}_1, \mathbf{y}_2, \mathbf{y}_3, \dots, \mathbf{y}_M\} \in \mathbb{R}^{D_2}$, which are views with bijective correspondence that were sampled from the same physical phenomena. The goal is to find a lower dimensional representation for each view that preserves the interactions between multidimensional data points and between the views \mathbf{X} and \mathbf{Y} .

A. Multiview Diffusion Maps

We begin by generalizing the DM framework for handling a multiview scenario. Our goal is to impose a random walk model using the local connectivities between data points within both views. Our way to incorporate the connectivities is by restraining the random walker to “hop” between views in each step. The first step in this construction is to choose a symmetrical and positive-semi-definite kernel functions one for each view: $\mathcal{K}^x : \mathbf{X} \times \mathbf{X} \rightarrow R$, and $\mathcal{K}^y : \mathbf{Y} \times \mathbf{Y} \rightarrow R$, as explained in Section II-B. A common choice is a Gaussian kernel. These kernels should capture the local intrinsic geometry of each view and neglect the global geometry. From \mathcal{K}^x and \mathcal{K}^y , we form a large row-stochastic matrix of size $2M \times 2M$ as follows: first we compute a matrix product $\mathbf{K}^z = \mathbf{K}^x \mathbf{K}^y$ between the kernels \mathcal{K}^x and \mathcal{K}^y such that (for a kernel)

$$K_{i,j}^z = \sum_m K_{i,m}^x K_{m,j}^y = \sum_m e^{-\frac{\|\mathbf{x}_i - \mathbf{x}_m\|^2}{2\sigma_x^2}} e^{-\frac{\|\mathbf{y}_m - \mathbf{y}_j\|^2}{2\sigma_y^2}} = [\mathbf{K}^z]_{i,j}, \quad (4)$$

then, the generalized multiview kernel is formed by the following matrix

$$\widehat{\mathbf{K}} = \begin{bmatrix} \mathbf{0}_{M \times M} & \mathbf{K}^z \\ (\mathbf{K}^z)^T & \mathbf{0}_{M \times M} \end{bmatrix}. \quad (5)$$

Finally, by using the diagonal matrix $\widehat{\mathbf{D}}, \widehat{D}_{i,i} = \sum_j \widehat{K}_{i,j}$, we compute the normalized row-stochastic matrix

$$\widehat{\mathbf{P}} = \widehat{\mathbf{D}}^{-1} \widehat{\mathbf{K}}, \quad \widehat{P}_{i,j} = \frac{\widehat{K}_{i,j}}{\widehat{D}_{i,i}}, \quad (6)$$

which describes the probability matrix of a Markov random walk between the data points of \mathbf{X} and \mathbf{Y} . The block anti diagonal form of $\widehat{\mathbf{K}}$ is symmetric, and the normalized version $\widehat{\mathbf{P}}$ provides a probabilistic interpretation to the construction (explained in III-C).

B. Alternative Multiview Approaches

We describe here two alternative existing methods for incorporating views. We do not analyze these approaches but use them only as references for comparisons in the experimental evaluations.

Hadarnard product (element wise):

Multiplying the kernel matrices \mathcal{K}^x and \mathcal{K}^y element wise $\mathbf{K}^\circ = \mathbf{K}^x \circ \mathbf{K}^y$, $K_{i,j}^\circ = K_{i,j}^x \cdot K_{i,j}^y$. Then normalizing by the sum of rows results in a row stochastic matrix \mathbf{P}° . Where \circ is the Hadarnard matrix product. This approach can be described in terms of the framework in [5].

Lemma 1. In the special case of a Gaussian kernel with $\sigma_x = \sigma_y$ in Eq. (4), the resulting matrix \mathbf{K}° is equal to the matrix \mathbf{K}^z constructed using the concatenated vector $\mathbf{z}_i = [\mathbf{x}_i^T, \mathbf{y}_i^T]^T$ from both views.

In more general cases, where σ is chosen as a vector and this vector is constructed as the concatenation of data from two views σ_x and σ_y . This approach, which corresponds to [5], uses the kernel \mathbf{K}° as a comparison to our method.

Additive kernel:

Define the sum of kernels by $K^+ = K^x + K^y$. This kernel is normalized by the sum of rows. This random walk sums the step probabilities from each view. This approach is computationally inexpensive in comparison to the other methods, however, it is unclear what data geometry it reveals. If noise exists in the sampled data, the new kernel K^+ will contain the sum of noises from both views. This approach was proposed in [12].

C. Probabilistic interpretation of \hat{P}

Under our proposed construction (Eqs. (4), (5) and (6)), the elements $[\hat{P}^t]_{i,j} = \hat{p}_t(x_i, x_j)$ denote for each $i, j \in [1, M]$ the transition probability from node x_i to node x_j in t time steps “hopping” between the views X and Y in each step. Note that due to the block-anti-diagonal block structure of \hat{K} , (and \hat{P}), then for odd values of t , this probability is zero. However, for even values of t , this probability is nonzero describing an even time transition from view X through view Y and back to X . In the same way, $[\hat{P}^t]_{i+M,j+M} = \hat{p}_t(y_i, y_j)$ denotes the transition probability from node y_i to node y_j ($i, j \in [1, M]$) in t time steps. Likewise, $[\hat{P}^t]_{i,j+M} = \hat{p}_t(x_i, y_j)$ denotes the transition probability from node x_i to node y_j ($i, j \in [1, M]$) in t time steps. Note that this probability is nonzero only for odd values of t . This probability takes into consideration all the various possibilities of crossing from node x_i to node y_j by propagating in view 1 and then in view 2. Figure 1 illustrates the multiview transition probabilities compared to a single view approach using two Swiss-roll manifolds.

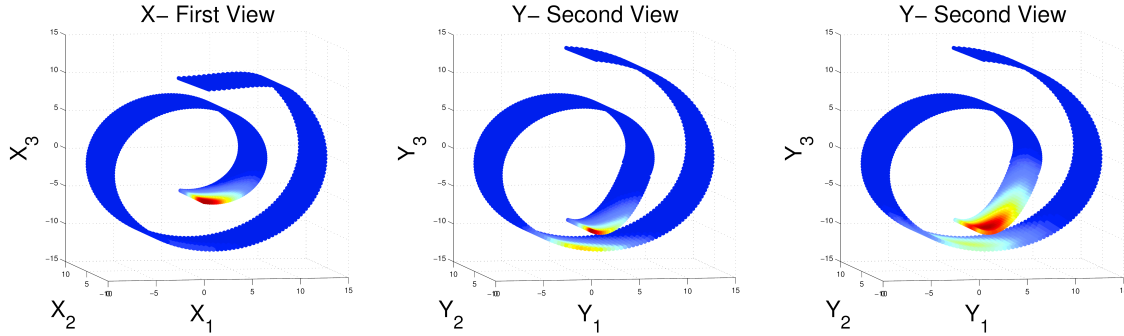


Fig. 1: Left: Swiss roll sampled from View-I (X), colored by the single view probability of transition ($t = 1$) from x_1 to x . Middle: second Swiss roll sampled from View-II (Y), colored by the single view probability of transition ($t = 1$) from y_1 to y . Right: the multiview probabilities of transition ($t = 1$) from x_i to y .

D. Spectral decomposition

In this section, we show how to compute the spectral decomposition of \hat{P} (Eq. (6)). The matrix \hat{P} is algebraically similar to the symmetric matrix \hat{P}_s since $\hat{P}_s = \hat{D}^{1/2} \hat{P} \hat{D}^{-1/2} = \hat{D}^{-1/2} \hat{K} \hat{D}^{-1/2}$. Therefore, both \hat{P} and \hat{P}_s share the same set of eigenvalues $\{\lambda_m\}$. Due to symmetry of the matrix \hat{P}_s , it has a set of $2M$ real eigenvalues $\{\lambda_i\}_{i=0}^{2M-1} \in \mathbb{R}$ and the corresponding real orthogonal eigenvectors $\{\pi_m\}_{m=0}^{2M-1} \in \mathbb{R}^{2M}$, thus, $\hat{P}_s = \Pi \Lambda \Pi^T$. By denoting $\Psi = \hat{D}^{-1/2} \Pi$ and $\Phi = \hat{D}^{1/2} \Pi$, we conclude that the set $\{\psi_m, \phi_m\}_{m=0}^{2M-1} \in \mathbb{R}^{2M}$ denotes the right and the left eigenvectors of $\hat{P} = \Psi \Lambda \Phi^T$, respectively, satisfying $\psi_i^T \phi_j = \delta_{ij}$. In the sequel, we use the symmetric matrix \hat{P}_s to simplify this analysis.

To avoid the spectral decomposition of a $M \times M$ matrix (\hat{P}_s), the spectral decomposition of \hat{P}_s can be computed using a Singular Value Decomposition (SVD) of the matrix $\bar{K}^z = D^{rows-1/2} K^z D^{cols-1/2}$ of size $M \times M$ where $D_{i,i}^{rows} = \sum_{j=1}^M K_{i,j}^z$ and $D_{j,j}^{cols} = \sum_{i=1}^M K_{i,j}^z$ are diagonal matrices. Theorem 4 enables us to form the eigenvectors of \hat{P} as a concatenation of the singular vectors of K^z (Eq. (4)).

Theorem 1. By using the left and right singular vectors of $K^z = V \Sigma U^T$, the eigenvectors and the eigenvalues of \hat{K} are computed explicitly by

$$\Pi = \frac{1}{\sqrt{2}} \begin{bmatrix} V & V \\ U & -U \end{bmatrix}, \Lambda = \begin{bmatrix} \Sigma & \mathbf{0}_{M \times M} \\ \mathbf{0}_{M \times M} & -\Sigma \end{bmatrix}. \quad (7)$$

Proof: Both V and U are orthonormal sets, therefore, $u_i^T u_j = \delta_{ij}$, and $v_i^T v_j = \delta_{ij}$, thus, the set $\{\pi_m\}$ is orthonormal therefore $\Pi \Pi^T = I$. By using the construction defined in Eq. (7), $\Pi \Lambda \Pi^T$ is computed explicitly by

$$\begin{aligned} \Pi \Lambda \Pi^T &= \frac{1}{2} \begin{bmatrix} V & V \\ U & -U \end{bmatrix} \begin{bmatrix} \Sigma & \mathbf{0} \\ \mathbf{0} & -\Sigma \end{bmatrix} \begin{bmatrix} V^T & U^T \\ V^T & -U^T \end{bmatrix} = \frac{1}{2} \begin{bmatrix} V \Sigma & -V \Sigma \\ U \Sigma & U \Sigma \end{bmatrix} \begin{bmatrix} V^T & U^T \\ V^T & -U^T \end{bmatrix} = \\ &= \frac{1}{2} \begin{bmatrix} \mathbf{0} & 2K^z \\ (2K^z)^T & \mathbf{0} \end{bmatrix} = \hat{K}. \mathbf{0} \text{ denotes the all zeros } M \times M \text{ matrix.} \end{aligned}$$

■

E. Multiview Diffusion Distance

In a variety of real life data types, the Euclidian distance does not provide a sufficient indication on the intrinsic relations between data points. The Euclidian distance is highly sensitive to scaling and rotations of multidimensional data points. Tasks such as classification, clustering or system identification require a measure for the intrinsic connectivity between data points. This type of measure is only satisfied locally by the Euclidian distance in the high dimensional ambient space. The multiview diffusion kernel (defined in section (III-A)) indicates about all the small local connections between data points. The row stochastic matrix $\hat{\mathbf{P}}^t$ (Eq. (6)) incorporates all the possibilities for having a transition in t time steps between data points that are hopping between both views. For a fixed value $t > 0$, two data points are *intrinsically similar* if the conditional distributions $\hat{\mathbf{p}}_t(\mathbf{x}_i, \cdot) = [\hat{\mathbf{P}}^t]_{i,\cdot}$ and $\hat{\mathbf{p}}_t(\mathbf{x}_j, \cdot) = [\hat{\mathbf{P}}^t]_{j,\cdot}$ are similar. This type of similarity measure indicates that the points \mathbf{x}_i and \mathbf{x}_j are similarly connected to several mutual points. Thus, they are connected by a geometrical path. In many cases, a small Euclidean distance could be misleading due to the fact that two data points could be “close” without having any Geodesic path that connects them. The similarity between probabilities is more robust in these cases.

Based on this observation, by expanding the single view construction given in [5], we define the weighted inner view diffusion distances to be

$$\mathcal{D}_t^2(\mathbf{x}_i, \mathbf{x}_j) = \sum_{k=1}^{2M} \frac{([\hat{\mathbf{P}}^t]_{i,k} - [\hat{\mathbf{P}}^t]_{j,k})^2}{\phi_o(k)} = \|(\mathbf{e}_i - \mathbf{e}_j)^T \hat{\mathbf{P}}^t\|_{\hat{\mathbf{D}}^{-1}}^2 \quad (8)$$

where \mathbf{e}_i is the i -th column of an $2M \times 2M$ identity matrix, ϕ_o is the first left eigenvector of $\hat{\mathbf{P}}$, its k -th element is $\phi_o(k) = \hat{D}_{k,k}$. The weighted norm on \mathbf{x} is defined as $\|\mathbf{x}\|_{\mathbf{W}}^2 = \mathbf{x}^T \mathbf{W} \mathbf{x}$. Similarly,

$$\mathcal{D}_t^2(\mathbf{y}_i, \mathbf{y}_j) = \sum_{k=1}^{2M} \frac{([\hat{\mathbf{P}}^t]_{M+i,k} - [\hat{\mathbf{P}}^t]_{M+j,k})^2}{\phi_o(k)} = \|(\mathbf{e}_{M+i} - \mathbf{e}_{M+j})^T \hat{\mathbf{P}}^t\|_{\hat{\mathbf{D}}^{-1}}^2. \quad (9)$$

The main advantage of these distance (Eqs. (8) and (9)) is that they can be expressed in terms of the eigenfunctions and the eigenvectors of the matrix $\hat{\mathbf{P}}$. This insight allows us to use a representation (defined in section III-F) in which the induced Euclidean distance is proportional to the diffusion distances (defined in Eqs. (8) and (9)).

Theorem 2. *The inner view diffusion distance defined by Eqs. (8) and (9) is equal to:*

$$\mathcal{D}_t^2(\mathbf{x}_i, \mathbf{x}_j) = 2 \cdot \sum_{\ell=1}^{M-1} \lambda_\ell^{2t} (\psi_\ell(i) - \psi_\ell(j))^2, i, j = 1, \dots, M, \quad (10)$$

and

$$\mathcal{D}_t^2(\mathbf{y}_i, \mathbf{y}_j) = 2 \cdot \sum_{\ell=1}^{M-1} \lambda_\ell^{2t} (\psi_\ell(M+i) - \psi_\ell(M+j))^2, i, j = 1, \dots, M. \quad (11)$$

Proof: We prove it for one view, the proof applies to the second view with proper adjustments. We can express $\hat{\mathbf{P}}^t \hat{\mathbf{D}}^{-1} (\hat{\mathbf{P}}^t)^T$ as $\hat{\mathbf{P}}^t \hat{\mathbf{D}}^{-1} (\hat{\mathbf{P}}^t)^T = \mathbf{\Psi} \mathbf{\Lambda}^t \mathbf{\Phi}^T \hat{\mathbf{D}}^{-1} \mathbf{\Phi} \mathbf{\Lambda}^t \mathbf{\Psi}^T = \mathbf{\Psi} \mathbf{\Lambda}^{2t} \mathbf{\Psi}^T$ since $\mathbf{\Phi}^T \hat{\mathbf{D}}^{-1} \mathbf{\Phi} = \mathbf{\Pi}^T \mathbf{\Pi} = \mathbf{I}$. Therefore, $\mathcal{D}_t^2(\mathbf{x}_i, \mathbf{x}_j) = \|(\mathbf{e}_i - \mathbf{e}_j)^T \hat{\mathbf{P}}^t\|_{\hat{\mathbf{D}}^{-1}}^2 = (\mathbf{e}_i - \mathbf{e}_j)^T \hat{\mathbf{P}}^t \hat{\mathbf{D}}^{-1} (\hat{\mathbf{P}}^t)^T (\mathbf{e}_i - \mathbf{e}_j) = (\mathbf{e}_i - \mathbf{e}_j)^T \mathbf{\Psi} \mathbf{\Lambda}^{2t} \mathbf{\Psi}^T (\mathbf{e}_i - \mathbf{e}_j) = \sum_{\ell=0}^{2M-1} \lambda_\ell^{2t} (\psi_\ell(i) - \psi_\ell(j))^2 = 2 \sum_{\ell=1}^{M-1} \lambda_\ell^{2t} (\psi_\ell(i) - \psi_\ell(j))^2$. Equality #5 is due to the repetitive form of $\hat{\mathbf{D}}$ and $\mathbf{\Pi}$ therefore of $\mathbf{\Psi}$ and $\mathbf{\Lambda}$, as described in Eq. (7). $\ell = 0$ is excluded due to the property of $\mathbf{\Psi}_0 = \mathbf{1}$ (an all-ones vector), which holds for all the stochastic matrices. ■

Using the inner view diffusion distances defined in Eqs. (8) and (9), we define a convex multiview diffusion distance as a convex linear combination of the inner views distances set by parameter $0 \leq \gamma \leq 1$ to be

$$\mathcal{D}_t^{(MV)}(i, j) = \gamma \|\Psi_t(\mathbf{x}_i) - \Psi_t(\mathbf{x}_j)\|^2 + (1 - \gamma) \|\Psi_t(\mathbf{y}_i) - \Psi_t(\mathbf{y}_j)\|^2. \quad (12)$$

By setting the parameter γ , we control the influence of each view on our induced distance measure. From the application point of view, this distance is useful given that one view is more reliable than the other.

F. Multiview data parametrization

Tasks such as classification, clustering or regression in a sampled high-dimensional feature space are considered to be computationally expensive. In addition, the performance of these tasks is highly dependent on the distance measure. As explained above, distance measures in the original ambient space are meaningless in many real life situations. Interpreting Theorem 2 in terms of Euclidean distance enables us to define two mappings for \mathbf{X} and \mathbf{Y} by using the right eigenvectors weighted by λ_ℓ^t . A representation for \mathbf{X} is given by

$$\Psi_t(\mathbf{x}_i) : \mathbf{x}_i \mapsto [\lambda_1^t \psi_1(i), \lambda_2^t \psi_2(i), \lambda_3^t \psi_3(i), \dots, \lambda_{M-1}^t \psi_{M-1}(i)]^T \in \mathbb{R}^{M-1} \quad (13)$$

and a representation for \mathbf{Y} is given by

$$\Psi_t(\mathbf{y}_i) : \mathbf{y}_i \mapsto [\lambda_1^t \psi_1(M+i), \lambda_2^t \psi_2(M+i), \lambda_3^t \psi_3(M+i), \dots, \lambda_{M-1}^t \psi_{M-1}(M+i)]^T \in \mathbb{R}^{M-1}. \quad (14)$$

These mappings capture the intrinsic geometry of both views as well as the mutual relation between the views. In section III-I, we showed that the set of eigenvalues λ_m has a decaying property such that $1 = |\lambda_0| \geq |\lambda_1| \geq \dots \geq |\lambda_{M-1}|$. Exploiting the decaying property enables us to represent data up to a dimension r such that $r \ll D_1, D_2$. The dimension $r \equiv r(\delta)$ is determined by approximating the diffusion distances (Eqs. (10) and (11)) up to a desired accuracy δ . This argument is expanded in section III-I.

G. Coupled mapping

The mapping provided by our approach is justified by the relations given by Eqs. (10) and (11). In this section, we provide another analytic justification for the proposed mapping. We start with an analysis of a 1-dimensional mapping for each view. Let $\rho(\mathbf{x}) = (\rho(\mathbf{x}_1), \rho(\mathbf{x}_2), \dots, \rho(\mathbf{x}_M))$ and $\rho(\mathbf{y}) = (\rho(\mathbf{y}_1), \rho(\mathbf{y}_2), \dots, \rho(\mathbf{y}_M))$ denote such mappings (one for each view), denote $\hat{\rho} \triangleq (\rho(\mathbf{x}), \rho(\mathbf{y}))$. Our mapping should preserve local connectivities, therefore, we want to ensure that if the points i and j are close in both views, then $\rho(\mathbf{x}_i), \rho(\mathbf{x}_j)$ and $\rho(\mathbf{y}_i), \rho(\mathbf{y}_j)$ will be close. Minimization of the following objective function

$$\underset{\hat{\rho}}{\operatorname{argmin}} \sum_{i,j} \left[(\rho(\mathbf{x}_i) - \rho(\mathbf{x}_j))^2 K_{i,j}^z + (\rho(\mathbf{y}_i) - \rho(\mathbf{y}_j))^2 (K_{i,j}^z)^T \right] \quad (15)$$

with mild additional constrains provides such connectivity preserving mapping. If $\hat{K}_{i,j}$ is small (indicating low connectivity between point i and j) the distance in the mappings could be large, on the other hand if $\hat{K}_{i,j}$ is large (indicating high connectivity between point i and j) the distance in the mappings will be small (to minimize the objective function).

Theorem 3. *Setting $\hat{\rho} = \psi_1$ minimizes the objective function in Eq. 15, where ψ_1 is the second eigenvector of the eigenvalue problem $\lambda_i \hat{\mathbf{P}} = \psi_i \hat{\mathbf{P}}$.*

$$\begin{aligned} \text{Proof: } \sum_{i,j} \left[(\rho(\mathbf{x}_i) - \rho(\mathbf{x}_j))^2 K_{i,j}^z + (\rho(\mathbf{y}_i) - \rho(\mathbf{y}_j))^2 K_{i,j}^z \right] &= \sum_{i,j} \rho(\mathbf{x}_i)^2 K_{i,j}^z + \sum_{i,j} \rho(\mathbf{x}_j)^2 (K_{i,j}^z)^T - \sum_{i,j} 2\rho(\mathbf{x}_i)\rho(\mathbf{x}_j)K_{i,j}^z + \\ \sum_{i,j} \rho(\mathbf{y}_i)^2 K_{i,j}^z + \sum_{i,j} \rho(\mathbf{y}_j)^2 (K_{i,j}^z)^T - \sum_{i,j} 2\rho(\mathbf{y}_i)\rho(\mathbf{y}_j)K_{i,j}^z &= \sum_i \rho(\mathbf{x}_i)^2 D_{i,i}^{\text{rows}} + \sum_j \rho(\mathbf{x}_j)^2 D_{j,j}^{\text{cols}} - \sum_{i,j} 2\rho(\mathbf{x}_i)\rho(\mathbf{x}_j)K_{i,j}^z + \\ \sum_i \rho(\mathbf{y}_i)^2 D_{i,i}^{\text{cols}} + \sum_j \rho(\mathbf{y}_j)^2 D_{j,j}^{\text{rows}} - \sum_{i,j} 2\rho(\mathbf{y}_i)\rho(\mathbf{y}_j)K_{i,j}^z &= \\ [\rho(\mathbf{x}) \quad \rho(\mathbf{y})] \left[\begin{bmatrix} D^{\text{rows}} & \mathbf{0}_{M \times M} \\ \mathbf{0}_{M \times M} & D^{\text{cols}} \end{bmatrix} - \begin{bmatrix} \mathbf{0}_{M \times M} & \mathbf{K}^z \\ (\mathbf{K}^z)^T & \mathbf{0}_{M \times M} \end{bmatrix} \right] \begin{bmatrix} \rho(\mathbf{x})^T \\ \rho(\mathbf{y})^T \end{bmatrix} \end{aligned}$$

adding a scaling constrain, we now rewrite the minimization problem as the following

$$\underset{\hat{\rho} \hat{\mathbf{D}} \hat{\rho}^T = 1}{\operatorname{argmin}} \hat{\rho} (\hat{\mathbf{D}} - \hat{\mathbf{K}}) \hat{\rho}^T, \quad (16)$$

this minimization problem can be solved by finding the minimum eigenvalue of $(\hat{\mathbf{D}} - \hat{\mathbf{K}}) \hat{\rho}^T = \bar{\lambda} \hat{\mathbf{D}} \hat{\rho}^T$. This eigenproblem has a trivial solution, an all ones eigenvector with $\bar{\lambda} = 0$. We add the following constraint $\hat{\rho} \hat{\mathbf{D}} \mathbf{1} = 0$ to remove the trivial solution. The solution is given by the smallest non zero eigenvalue, multiplying the equation by $\hat{\mathbf{D}}^{-1}$ reduces the problem to the following $\hat{\rho} \hat{\mathbf{P}} = \lambda \hat{\mathbf{P}}$, thus we are looking for the eigenvector which corresponds to the second largest eigenvalue. ■

H. Cross View Diffusion Distance

In some real-world physical systems, the observed dataset denoted by \mathbf{X} changes over some underlying parameter denoted by α . Under this model, we can obtain multiple snapshots for various values of α . Each snapshot is denoted by \mathbf{X}_α . If these datasets are high dimensional, quantifying the amount of change of the datasets is a difficult task. This scenario was recently studied in [19] by generalizing the diffusion framework for cases in which the data changes over the parameter α . An example of such a scenario occurs in hyper-spectral images that change over time. The DM framework is applied in [19] to every fixed value of α . Then, by using the extracted low dimensional mapping, the Euclidian distance enables to quantify the amount of change over α . This approach is sensitive since every small change in the data can result in different mappings and the mappings are extracted independently. Thus, there is no mutual influence on the extracted mapping. Our approach incorporates the mutual relations of data within the view and the relations among views. This observation enables us to measure in a more robust way the number of variations between two datasets that correspond to a small variation in α . We now define a new

diffusion distance. This distance measures the relation between two views, i.e. between all the data points. We measure the distance between all the coupled data points among both mappings by using the following expression:

$$\mathcal{D}_t^{(CM)^2}(X, Y) = \sum_{i=1}^{M-1} \|\Psi_t(\mathbf{x}_i) - \Psi_t(\mathbf{y}_i)\|^2. \quad (17)$$

Our kernel matrix is a product of the Gaussian kernel matrices in each view. If these values of the kernel matrices ($\mathbf{K}^x, \mathbf{K}^y$) are similar, this corresponds to similarity between the views inner geometry, and the right and left singular vectors of the matrix $\mathbf{K}^x \mathbf{K}^y$ will be similar, thus $\mathcal{D}_t^{(CM)}$ will be small.

Theorem 4. *The cross manifold distance (Eq. 17) is invariant to orthonormal transformations between the ambient spaces X and Y .*

Proof: Denote some orthonormal transformation matrix $\mathbf{R} : X \rightarrow Y$, w.l.o.g. $\mathbf{y}_i = \mathbf{R}\mathbf{x}_i$.
 $K_{i,j}^y = \exp\{-\frac{\|\mathbf{y}_i - \mathbf{y}_j\|^2}{2\sigma_y^2}\} = \exp\{-\frac{\|\mathbf{R}\mathbf{x}_i - \mathbf{R}\mathbf{x}_j\|^2}{2\sigma_y^2}\} = \exp\{-\frac{\|\mathbf{x}_i - \mathbf{x}_j\|^2}{2\sigma_x^2}\} = K_{i,j}^x$, the last equality is due to the orthonormality of \mathbf{R} and choosing $\sigma_y = \sigma_x$. Therefore, the matrix $\mathbf{K}^z = (\mathbf{K}^x)^2$ (Eq. 4) is symmetric and its right and left singular vectors are equal ($\mathbf{U} = \mathbf{V}$, Eq.(7)). This creates a repetitive form in $\Psi = \hat{\mathbf{D}}^{-1/2} \mathbf{\Pi} \rightarrow \psi_l(i) = \psi_l(M+i)$, $1 \leq i, l \leq M-1 \rightarrow \Psi_t(\mathbf{y}_i) = \Psi_t(\mathbf{x}_i)$, and thus, $\mathcal{D}_t^{(CM)^2}(X, Y) = 0$. ■

I. Spectral Decay of $\hat{\mathbf{K}}$

The power of kernel based methods for dimensionality reduction stems from the spectral decay of the kernel's eigenvalues. In this section, we study the relation between the spectral decay of a Gaussian kernel and our multiview generalized kernel's decay rate. In section V-B, we evaluate the spectral decay empirically using two experiments. The rest of this section is devoted to theoretical justification for the spectral decay of our proposed framework. We start with some background.

Theorem 5. *The eigenvalues of $\hat{\mathbf{P}}$ (Eq. 6) are real and bounded where $|\lambda_i| \leq 1$, $i = 1, \dots, 2M$.*

A similar proof is given in [20].

Proof: As shown in section III-D, $\hat{\mathbf{P}}$ is algebraically similar to a symmetric matrix, thus, its eigenvalues are guaranteed to be real. Denote by λ and ψ the eigenvalue and the eigenvector, respectively, such that $\lambda\psi = \hat{\mathbf{P}}\psi$. Define $i_0 = \underset{1 \leq i \leq 2M}{\operatorname{argmax}} |\psi(i)|$ to be the index of the largest entry in ψ . The maximal value $\psi(i_0)$ can be computed using $\hat{\mathbf{P}}$ from (Eq. 6) such that $\lambda\psi(i_0) = \sum_{j=1}^{2M} \hat{P}_{i_0j} \psi(j) \rightarrow |\lambda| = |\sum_{j=1}^{2M} \hat{P}_{i_0j} \frac{\psi(j)}{\psi(i_0)}| \leq \sum_{j=1}^{2M} \hat{P}_{i_0j} \frac{|\psi(j)|}{|\psi(i_0)|} \leq \sum_{j=1}^{2M} \hat{P}_{i_0j} = 1$. The first inequality is due to the triangle inequality and the second equality is due to the kernel normalization by $\hat{\mathbf{D}}^{-1}$. ■

The theorem shows that the eigenvalues are bounded. However, bounded eigenvalues are insufficient for dimensionality reduction. Dimensionality reduction is meaningful when there is a significant spectral decay.

Definition 1. *Let \mathcal{M} be a manifold. The intrinsic dimension d of the manifold is a positive integer determined by how many independent “coordinates” are needed to describe \mathcal{M} . Using a parametrization to describe a manifold, the dimension of \mathcal{M} is the smallest integer d such that a smooth map $\mathbf{f}(\xi) = \mathcal{M}$, $\xi \in \mathcal{R}^d$, describes the manifold, where $\xi \in \mathcal{R}^d$.*

Our framework is based on a Gaussian kernel. The spectral decay of Gaussian kernels was studied in [5], we use their following lemma.

Lemma 2. *Assume that the data is sampled from some manifold with intrinsic dimension $d \ll M$. Let \mathbf{K}° (section III-B) denotes a kernel with an exponential decay as a function of the Euclidean distance. For $\delta > 0$, the number of eigenvalues of \mathbf{K}° above δ is proportional to $(\log(\frac{1}{\delta}))^d$.*

Lemma 2 is based on Weyl's asymptotic law [21]. Let $r_\delta = r(\delta) = \max\{\ell \in N \text{ such that } |\lambda_\ell| \geq \delta\}$ denotes the number of eigenvalues of \mathbf{K}° above δ . $K_{i,j}^\circ = K_{i,j}^x K_{i,j}^y$ corresponds to a single DM view given in [5]. Theorem 6 relates the spectral decay of the proposed framework in [5].

Lemma 3. *Let $\mathbf{X}, \mathbf{Y} \in \mathbb{R}^{M \times M}$ such that $\mathbf{X}, \mathbf{Y} \geq 0$. Then for any $1 \leq k \leq M-1$*

$$\prod_{\ell=k}^{M-1} \lambda_\ell(\mathbf{X}\mathbf{Y}) \leq \prod_{\ell=k}^{M-1} \lambda_\ell(\mathbf{X} \circ \mathbf{Y}) \quad (18)$$

where \circ is the Kronecker matrix product.

This inequality is proved in [22] and [23].

Theorem 6. *Multiplying the last $M-1-r_\delta$ eigenvalues of \mathbf{K}^z is smaller than δ^{M-1-r_δ} . Formally, $\prod_{\ell=r_\delta}^{M-1} \lambda_\ell(\mathbf{X}\mathbf{Y}) \leq \delta^{M-1-r_\delta}$.*

Proof:

Denote by $\{\lambda_i(\mathbf{X})\}_{i=0}^{M-1}$ the eigenvalues of a matrix \mathbf{X} . They are enumerated in descending order such that $\lambda_0(\mathbf{X}) \geq \lambda_1(\mathbf{X}) \geq \dots \geq \lambda_{M-1}(\mathbf{X})$. We use Lemma 3 to prove Theorem 6, by choosing $\mathbf{X} = \mathbf{K}^x, \mathbf{Y} = \mathbf{K}^y$, which are positive semi-definite, $\mathbf{K}^x \circ \mathbf{K}^y = \mathbf{K}^\circ$ corresponds to Lafon's approach [5]. By using Lemma 3 and choosing $\ell = r_\delta$ in Eq. 18, we get

$$\prod_{\ell=r_\delta}^{M-1} \lambda_\ell(\mathbf{K}^x \mathbf{K}^y) \leq \prod_{\ell=r_\delta}^{M-1} \lambda_\ell(\mathbf{K}^\circ) \leq \delta^{M-1-r_\delta}.$$

■

Using the kernel matrix spectral decay, we can approximate Eqs. (10) and (11) by neglecting all the eigenvalues that are smaller than δ . Thus, we can compute a low dimensional mapping such that

$$\hat{\Psi}_t^r(\mathbf{x}_i) : \mathbf{x}_i \mapsto [\lambda_1^t \psi_1(i), \lambda_2^t \psi_2(i), \lambda_3^t \psi_3(i), \dots, \lambda_{r-1}^t \psi_{r-1}(i)]^T \in \mathbb{R}^{r-1}. \quad (19)$$

This mapping of dimension r provides a low dimensional space which improves the performance and efficiency of various Machine Learning tasks.

J. More than two views

In this paper, we focus on the coupled views scenario, however this approach can be applied to more views. In this section, we present the algebraic steps required when more than two views are present. Denoting the l -th view $\mathbf{X}^l, l = 1, \dots, L$, each view is a high dimensional dataset $\mathbf{X}^l = \{\mathbf{x}_1^l, \mathbf{x}_2^l, \mathbf{x}_3^l, \dots, \mathbf{x}_M^l\} \in \mathbb{R}^{M \times N}$. As presented in Section III-A the first step is to choose symmetrical positive semi definite kernels for each view $\mathcal{K}^l : \mathbf{X}^l \times \mathbf{X}^l \rightarrow \mathbb{R}, l = 1, \dots, L$, then the generalized multiview kernel is formed by the following matrix

$$\widehat{\mathbf{K}} = \begin{bmatrix} \mathbf{0}_{M \times M} & \mathbf{K}^1 \mathbf{K}^2 & \mathbf{K}^1 \mathbf{K}^3 & \dots & \mathbf{K}^1 \mathbf{K}^p \\ \mathbf{K}^2 \mathbf{K}^1 & \mathbf{0}_{M \times M} & \mathbf{K}^2 \mathbf{K}^3 & \dots & \mathbf{K}^2 \mathbf{K}^p \\ \mathbf{K}^3 \mathbf{K}^1 & \mathbf{K}^3 \mathbf{K}^2 & \mathbf{0}_{M \times M} & \dots & \mathbf{K}^3 \mathbf{K}^p \\ \vdots & \vdots & \vdots & \dots & \vdots \\ \mathbf{K}^p \mathbf{K}^1 & \mathbf{K}^p \mathbf{K}^2 & \mathbf{K}^p \mathbf{K}^3 & \dots & \mathbf{K}^p \mathbf{K}^p \end{bmatrix}, \quad (20)$$

then, by using the diagonal matrix $\widehat{\mathbf{D}}, \widehat{D}_{i,i} = \sum_j \widehat{K}_{i,j}$, we compute the normalized row-stochastic matrix

$$\widehat{\mathbf{P}} = \widehat{\mathbf{D}}^{-1} \widehat{\mathbf{K}}, \quad \widehat{P}_{i,j} = \frac{\widehat{K}_{i,j}}{\widehat{D}_{i,i}}, \quad (21)$$

where the m, l block (square $M \times M$ matrix located at $[1 + (m-1)M, 1 + (l-1)M], l = 1, \dots, L$) describes the probability of transition between view \mathbf{X}^m and \mathbf{X}^l . As explained in section III-D, the eigenvalues of the matrix $\widehat{\mathbf{P}}$ could be computed using the SVD of the block matrices, therefore $p-1$ decompositions are needed for each of the $M \times M$ block.

IV. INFINITESIMAL GENERATOR

In [5], a family of diffusion operators was introduced. Each of the operators differs by the normalization. Lafon and Coifman [5] prove that if appropriate limits are taken, $M \rightarrow \infty, \epsilon \rightarrow 0, \epsilon = 2\sigma^2$, the DM kernel operator will converge to one of the following differential operators: 1. Normalized graph Laplacian. 2. Laplace Beltrami diffusion. 3. Heat kernel equation. These are all special cases of the diffusion equation. This not only provides a physical justification for the DM framework, but allows in some cases to distinguish between the geometry and the density of the data points. In this section, we study the asymptotics of the proposed kernel $\widehat{\mathbf{K}}$ (Eq. 5).

Theorem 7. *The infinitesimal generator induced by our proposed kernel $\widehat{\mathbf{K}}$ (Eq. 5) converges when $M \rightarrow \infty, \epsilon \rightarrow 0, \epsilon = 2\sigma^2$ to a “cross domain Laplacian operator”. The functions $f(x)$ and $g(y)$ operate on the two manifolds \mathcal{M}_x and \mathcal{M}_y and are solutions to the following diffusion like equations:*

$$\begin{aligned} g(y) &= [m_1 f(y) + m_2 f''(y)], \\ f(x) &= [m_3 g(x) + m_4 g''(x)]. \end{aligned}$$

Proof: Assume x_1, x_2, \dots, x_M are i.i.d uniformly distributed on some manifold \mathcal{M}_x , and y_1, y_2, \dots, y_M are i.i.d uniformly distributed on another manifold \mathcal{M}_y . We use the functions $f(x)$ and $g(y)$ to construct the following vector

$$\mathbf{h} = [f(x_1), f(x_2), \dots, f(x_M), g(y_1), g(y_2), \dots, g(y_M)] \in \mathbb{R}^{2M}.$$

The limit of the characteristic equation is

$$\lim_{\substack{M \rightarrow \infty \\ \epsilon = \sigma_x = \sigma_y \rightarrow 0}} g(y_i) - \frac{\sum_{j=1}^M K_{ij}^z f(x_j)}{\sum_{j=1}^M K_{ij}^z} = \lim_{\substack{M \rightarrow \infty \\ \epsilon \rightarrow 0}} g(y_i) - \frac{\sum_{j=1}^M \sum_{l=1}^M e^{-\frac{\|x_i - x_l\|^2}{2\sigma_x^2}} e^{-\frac{\|y_l - y_j\|^2}{2\sigma_y^2}} f(x_j)}{\sum_{j=1}^M K_{ij}^z}.$$

The sum is approximated using a the following Riemann based integral

$$\frac{1}{M} \sum_{j=1}^M \sum_{l=1}^M e^{-\frac{\|x_i - x_l\|^2}{2\sigma_x^2}} e^{-\frac{\|y_l - y_j\|^2}{2\sigma_y^2}} f(x_j) \xrightarrow{M \rightarrow \infty} \int \int e^{-\frac{(y-t)^2}{2\sigma_y^2}} e^{-\frac{(x-t)^2}{2\sigma_x^2}} f(x) dx dt.$$

We use the following change of variables $z = \frac{x-t}{\sigma_x}$, $x = z\sigma_x + t$, $dx = dz\sigma_x$, to get

$$\int \int e^{-\frac{(y-t)^2}{2\sigma_y^2}} e^{-\frac{(x-t)^2}{2\sigma_x^2}} f(x) dx dt = \sigma_x \int \int e^{-\frac{z^2}{2}} e^{-\frac{(t-y)^2}{2\sigma_y^2}} f(t + z\sigma_x) dz dy.$$

By using Taylor's approximation of f we get

$$\begin{aligned} &= \sigma_x \int \int e^{-\frac{z^2}{2}} e^{-\frac{(t-y)^2}{2\sigma_y^2}} [f(t) + f'(t)z\sigma_x + \frac{1}{2}f''(t)z^2\sigma_x^2 + \dots] dz dy \\ &\approx \sigma_x \int e^{-\frac{(t-y)^2}{2\sigma_y^2}} [\int e^{-\frac{z^2}{2}} f(t) + \int e^{-\frac{z^2}{2}} f'(t)z\sigma_x + \frac{1}{2} \int e^{-\frac{z^2}{2}} f''(t)z^2\sigma_x^2] dz dy \\ &= \sigma_x \int e^{-\frac{(t-y)^2}{2\sigma_y^2}} [a_0 f(t) + \frac{1}{2}a_1 f''(t)\sigma_x^2] dz dy, \end{aligned}$$

where $a_0 = \int e^{-\frac{z^2}{2}} dz = \sqrt{2\pi}$, $\int e^{-\frac{z^2}{2}} z dz = 0$ and $a_1 = \int e^{-\frac{z^2}{2}} z^2 dz = \sqrt{2\pi}$.

By another change of variables, $r = \frac{t-y}{\sigma_y}$, $t = r\sigma_y + y$, $dt = dr\sigma_y$, we get

$$\begin{aligned} &= \sigma_x \int e^{-\frac{r^2}{2}} [a_0 f(y + r\sigma_y) + \frac{1}{2}a_1 f''(y + r\sigma_y)\sigma_x^2] dr \\ &\approx \sigma_x \int e^{-\frac{r^2}{2}} [a_0 [f(y) + f'(y)r\sigma_y + \frac{1}{2}f''(y)r^2\sigma_y^2] + \frac{1}{2}a_1 \sigma_x^2 [f''(y) + f'''(y)r\sigma_y + \frac{1}{2}f''''(y)r^2\sigma_y^2]] dr \\ &\approx \sigma_x [a_0 \int e^{-\frac{r^2}{2}} f(y) dr + \frac{1}{2} \int e^{-\frac{r^2}{2}} f''(y)(r^2\sigma_y^2 + a_1 \sigma_x^2) dr] \\ &= \sigma_x [a_0^2 f(y) + a_3 f''(y)], \end{aligned}$$

where $a_3 = \int e^{-\frac{r^2}{2}} (r^2\sigma_y^2 + a_1 \sigma_x^2) dr = \sqrt{2\pi}(\sigma_y^2 + \sigma_x^2)$. We neglected order σ^4 terms. In the same way we compute the eigenfunctions $g(x)$

$$f(x) = \sigma_y [a_0^2 g(x) + a_4 g''(x)].$$

■

This infinitesimal generator is a coupled Laplacian operator acting on the manifolds. The characteristic functions induced by this operator are sines and cosines, just as in the standard diffusion equation.

V. EXPERIMENTAL RESULTS

In this section we present experiments which evaluate our framework for various purposes. The first experiment demonstrates the power of our method for spectral clustering. The second experiment evaluates the spectral decay rate of our proposed method. The third experiment evaluates the cross domain diffusion distance. The fourth experiment demonstrates how our proposed approach extracts coupled embeddings from coupled views. The final experiment demonstrates the proposed approach on a real data set.

A. Experiment I- Spectral Clustering

Spectral properties of data sets are useful in the context of clustering, as they reveal information regarding the unknown number of clusters. The characteristic of the eigenvalues could provide insight on the number of clusters within the data set. A study by Ng et al. [24] relates the number of clusters to the multiplicity of the eigenvalue 1. A different approach by Perona

[25], provides an analysis for the relation between the eigenvalue drop to the number of clusters. In this section, we evaluate how our proposed method captures the clusters' structure when two views are available.

We generate two circles representing the original clusters, using the following function

$$\mathbf{Z} = \begin{bmatrix} z_i^1 \\ z_i^2 \end{bmatrix} = \begin{bmatrix} r \cos(\theta_i) \\ r \sin(\theta_i) \end{bmatrix}, \quad (22)$$

where $\theta_i, 1 \leq i \leq 1600$ are 1600 points spread linearly within the line $[0, 4\pi]$, the clusters are created by changing the radius as follows $r = 2.2, 1 \leq i \leq 800$ (first cluster), $r = 4, 801 \leq i \leq 1600$ (second cluster). The views \mathbf{X}, \mathbf{Y} are generated by applying the following non linear functions to generate distorted views

$$x_i^1 = \begin{cases} z_i^1 + 0.8 + n_i^2 |z_i^2| \geq 0 \\ z_i^1 - 0.8 + n_i^3 |z_i^2| \leq 0 \end{cases}, x_i^2 = z_i^2 + n_i^1 \quad (23)$$

$$y_i^1 = z_i^1 + n_i^4, y_i^2 = \begin{cases} z_i^2 + 0.8 + n_i^5 |z_i^1| \geq 0 \\ z_i^2 - 0.8 + n_i^6 |z_i^1| \leq 0 \end{cases}, \quad (24)$$

where $n_i^l, 1 \leq l \leq 6$ are i.i.d random variables drawn from a Gaussian distribution with $\mu = 0, \sigma_n = 0.35$.

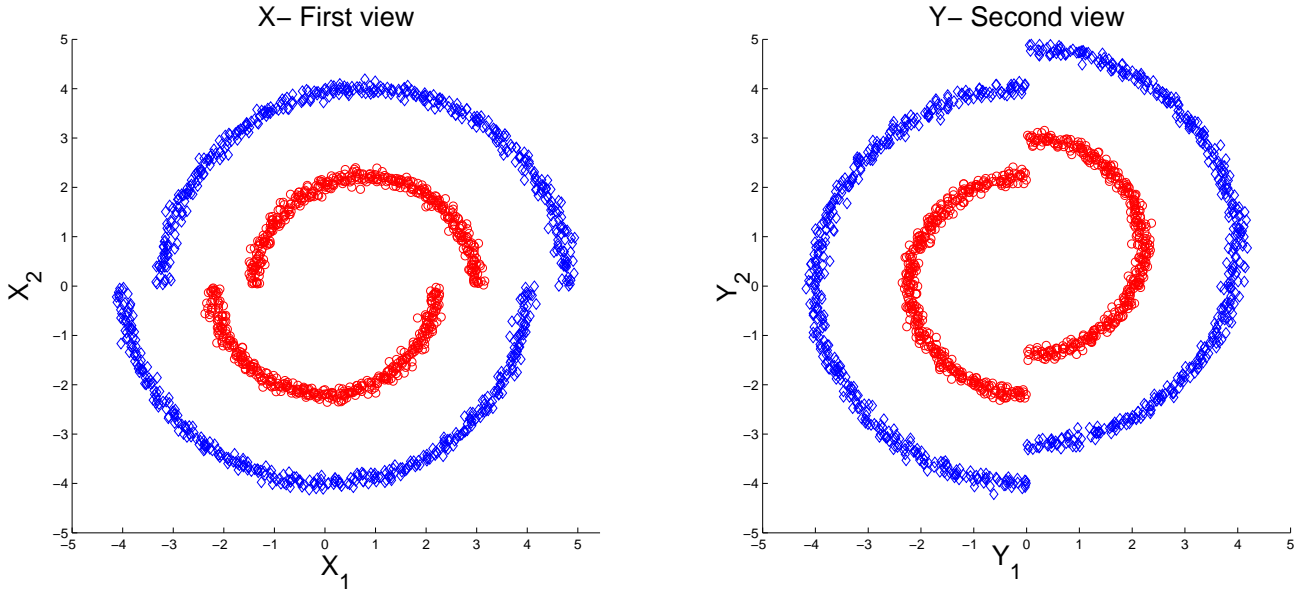


Fig. 2: Both views \mathbf{X}, \mathbf{Y} , marker color and shape represent the original clusters

In figure 2 the views \mathbf{X}, \mathbf{Y} generated using Eqs. (23) and (24) are presented. We first apply DM to each view and perform clustering using K-means within the first diffusion coordinate. We use the following parameters $t = 1, \sigma_x = \sigma_y = 0.05, k = 1$. The results are presented in figure 3. We apply the proposed multiview framework and kernel product DM based on both views, and finally apply K-means to the first extracted diffusion coordinate. For the multiview experiment we use the following parameters $t = 1, \sigma_x = \sigma_y = 0.05, \sigma^\circ = 0.071, k = 1$. the results are presented in figure 4. It is evident that our approach outperforms the single view DM and the Kernel Product approaches. To evaluate the performance of our proposed mapping, we perform 100 simulation for various values of the Gaussian's noise variance (all with zero mean), the average clustering success rate is presented in Fig. 5.

B. Experiment II- Spectral Decay

In Section III-I we presented an upper bound on the eigenvalues' decay rate of our proposed method. In order to empirically evaluate the decay rate, we generate artificial datasets and compare our method to other approaches. We evaluate the spectral decay of our proposed framework (MultiView Diffusion), Lafon's approach [5] (Kernel Product) and the summation approach (Kernel Sum). We compare the frameworks on artificial clustered data drawn from Gaussian distributions. The following steps describe the generation of both views, denoted as (\mathbf{X}, \mathbf{Y}) referred as View-I (\mathbf{X}) and View-II (\mathbf{Y}) respectively.

- 1) Draw six vectors ($1 \leq j \leq 6 | \boldsymbol{\mu}_j \in \mathbb{R}^9$) from a Gaussian distribution $N(\mathbf{0}, 8 \cdot \mathbf{I}_{9 \times 9})$, these vectors are the center of masses for the generated classes.

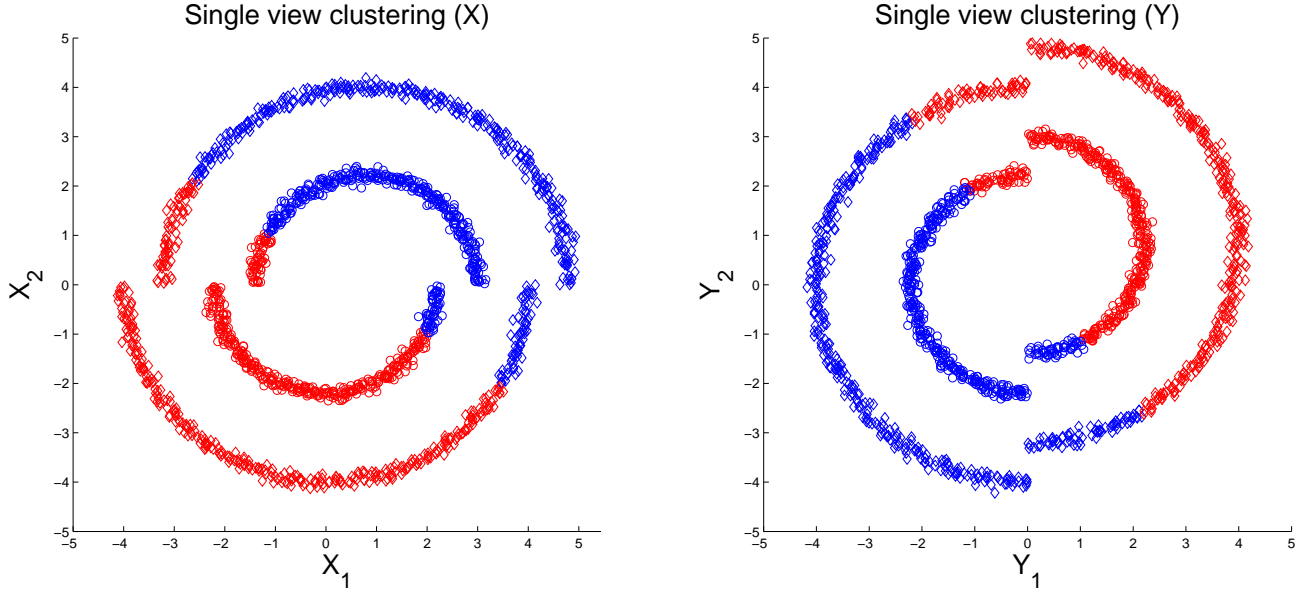


Fig. 3: Marker color - clustering results based on a single view, marker shape- ground truth

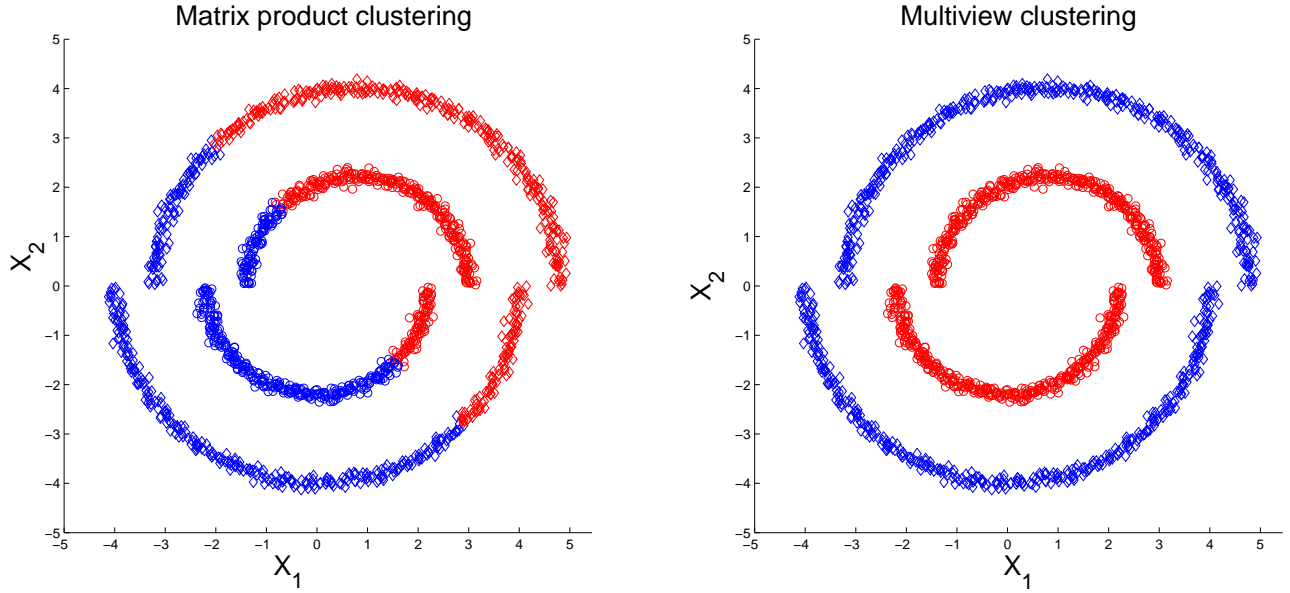


Fig. 4: Marker color - clustering results based on a multiview (left) and based on kernel product (right), marker shape- ground truth cluster number

- 2) Draw 100 data points for each cluster j , using $\mu_j, 1 \leq j \leq 6$ from another Gaussian distribution $N(\mu_j, 2 \cdot \mathbf{I}_{9 \times 9})$. Denote these 600 data points as \mathbf{X} .
- 3) Draw 100 data points for each cluster j , using $\mu_j, 1 \leq j \leq 6$ from another Gaussian distribution $N(\mu_j, 2 \cdot \mathbf{I}_{9 \times 9})$. Denote these 600 data points as \mathbf{Y} .

The first 3 dimensions of both views are presented in Fig. 6. We compute the probability matrix for each view ($\mathbf{P}^x, \mathbf{P}^y$), the kernel sum approach probability matrix (\mathbf{P}^s), the concatenation approach (\mathbf{P}^o) and the multiview diffusion approach ($\hat{\mathbf{P}}$). We compute the eigendecomposition of all matrices, compare all of the resulting eigenvalues decay rate to the eigenvalues product from both views (a stronger decay than each view separately). To have a fair comparison between all the above methods, we chose the Gaussian scale parameter for each view σ_x, σ_y , and used the same scales for all methods. The vectors' variance in the concatenation approach is the sum of the variances (assuming statistical independence); therefore, we use the following scale parameters $\sigma_o^2 = \sigma_x^2 + \sigma_y^2$. We repeat this experiment but this time \mathbf{X} consists of 6 clusters, whereas \mathbf{Y} only 3. For \mathbf{Y} we use only the first center of masses and generating 200 points in each cluster. Figure 7 presents a logarithmic scale of the

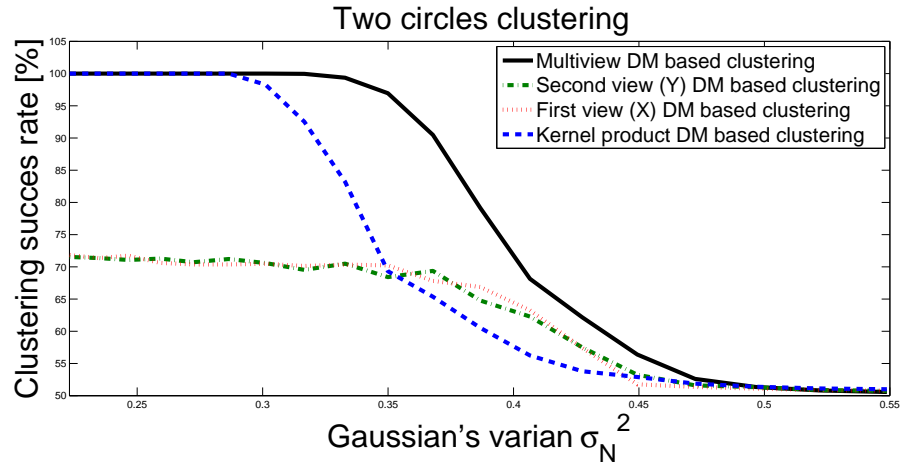


Fig. 5: Clustering success rate vs. the variance of the Gaussian noise, simulated on the two circles coupled views dataset.

spectral decay for eigenvalues extracted from various methods. It is evident that our proposed kernel has the strongest spectral decay.

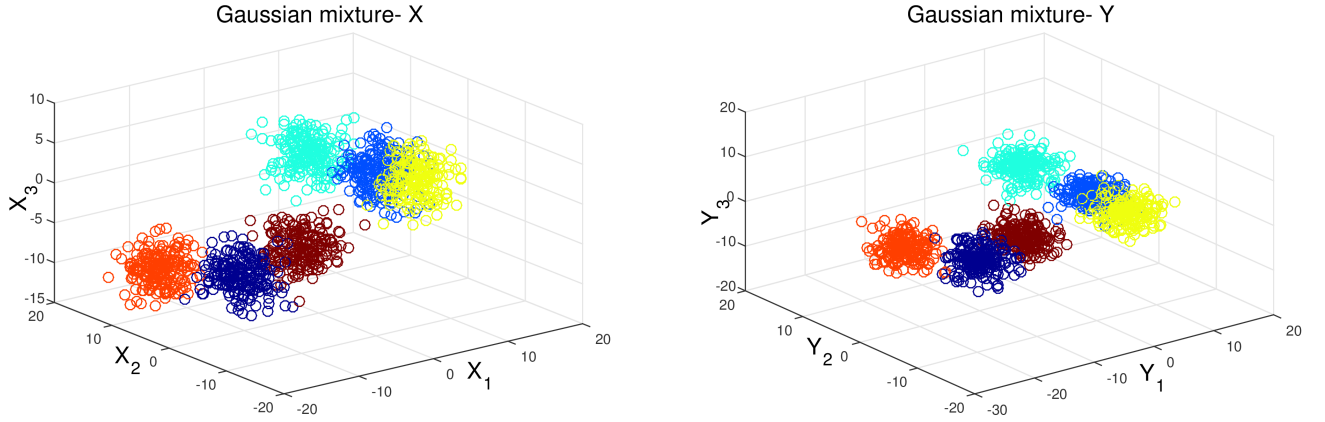


Fig. 6: First 3 dimensions of the Gaussian mixture, both views share the center of masses of the Gaussian spread. Left- first view denoted as X , Right- second view denoted as Y . The variance of the Gaussian in each dimension is 8.

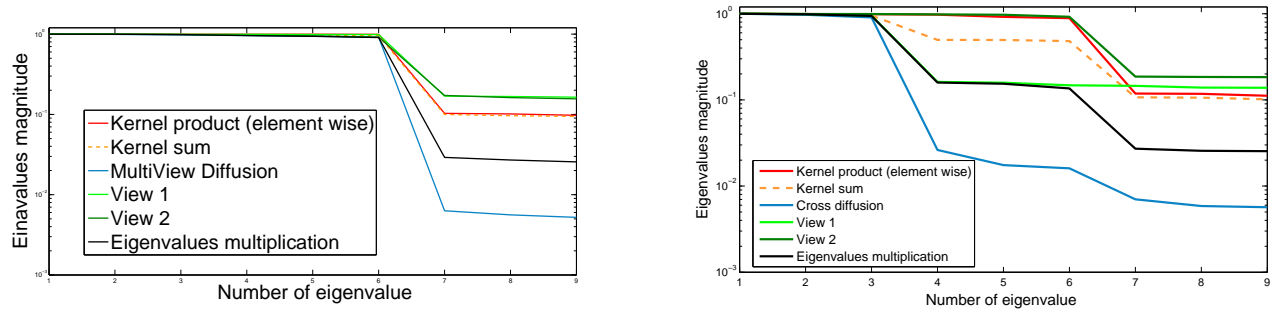


Fig. 7: Eigenvalues decay rate, comparison between the different mapping methods. Left- 6 clusters in each view, right- 6 clusters in X , 3 clusters in Y .

C. Experiment III- Cross View Diffusion Distance

In this section we examine the proposed Cross View Diffusion Distance (Section III-H). We generate a swiss roll using the following function

$$\text{View I: } \mathbf{X} = \begin{bmatrix} x_i^1 \\ x_i^2 \\ x_i^3 \end{bmatrix} = \begin{bmatrix} 6\theta_i \cos(\theta_i) \\ h_i \\ 6\theta_i \sin(\theta_i) \end{bmatrix} + \mathbf{N}_i^1 \quad (25)$$

$\theta_i = (1.5\pi)s_i$, $i = 1, 2, 3, \dots, 1000$, where s_i are 1000 data points spread linearly within the following line $s_i \rightarrow [1, 3]$. The second view is generated by applying an orthonormal transformation to the swiss roll and adding Gaussian noise. The following function describes the representation of the second view

$$\text{View II: } \mathbf{Y} = \begin{bmatrix} y_i^1 \\ y_i^2 \\ y_i^3 \end{bmatrix} = \mathbf{R} \begin{bmatrix} 6\theta_i \cos(\theta_i) \\ h_i \\ 6\theta_i \sin(\theta_i) \end{bmatrix} + \mathbf{N}_i^2 \quad (26)$$

where $\mathbf{R} \in \mathbb{R}^{3 \times 3}$ is a random orthonormal transformation matrix, it is generated by drawing values from i.i.d Gaussian variables and applying Gram-Schmidt processes. An example of both swiss rolls is presented in Fig. 8. We apply DM on each view

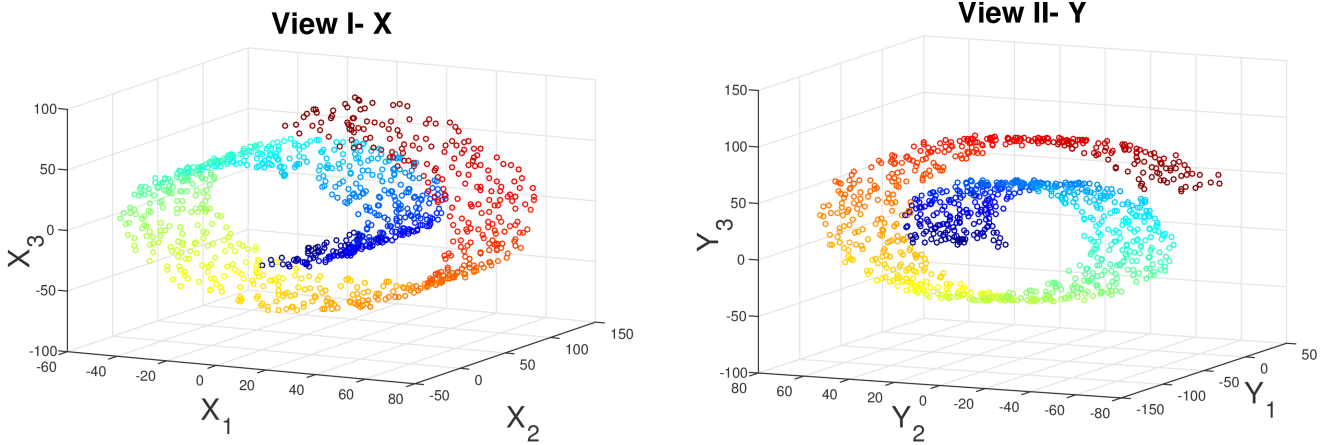


Fig. 8: The two Swiss Rolls generated using Eqs. (25) and (26).

and extract the embedding for the swiss roll, the sum of distances between all points in the embedding spaces is denoted as single view diffusion distance (SVDD). We apply the proposed framework to extract the coupled embedding, the Cross View Diffusion Distance (CVDD) is computed using Eq. (17). We run this experiment 100 times for various values of the Gaussian noise Variance. The median of the results are presented in Fig. 9. We use the median because in about 10% of the single view simulations the embedding are flipped, this causes a large SVDD although the embeddings share similar structures.

D. Experiment IV- Coupled Manifold Learning

DM is a powerful method for many applications, it is most powerful when the sampled high dimensional dataset lies on a lower dimensional manifold. In the general DM approach, there is an assumption that the sampled space describes one lower dimensional manifold, but this assumption could be flawed, and the sampled space could describe a redundancy in the manifold, or more generally, the sampled space could describe two or more manifolds generated by a common physical process. In this section, we examine the extracted embedding computed using our method and compare it to the Kernel Product approach (section III-B).

Helix A

We generate two coupled manifolds with a common underlying open circular structure. The helix shaped manifolds were generated by applying a 3 dimensional function to 1000 data points spread linearly within the following lines $a_i \rightarrow [0, 2\pi]$, $b_i = a_i + 0.5\pi \bmod 2\pi$, where $i = 1, 2, 3, \dots, 1000$. We use the following functions to generate the datasets for View-I and View-II (denoted as \mathbf{X} and \mathbf{Y} respectively)

$$\text{View I: } \mathbf{X} = \begin{bmatrix} x_i^1 \\ x_i^2 \\ x_i^3 \end{bmatrix} = \begin{bmatrix} 4 \cos(0.9a_i) + 0.3 \cos(20a_i) \\ 4 \sin(0.9a_i) + 0.3 \sin(20a_i) \\ 0.1(6.3a_i^2 - a_i^3) \end{bmatrix} \quad (27)$$

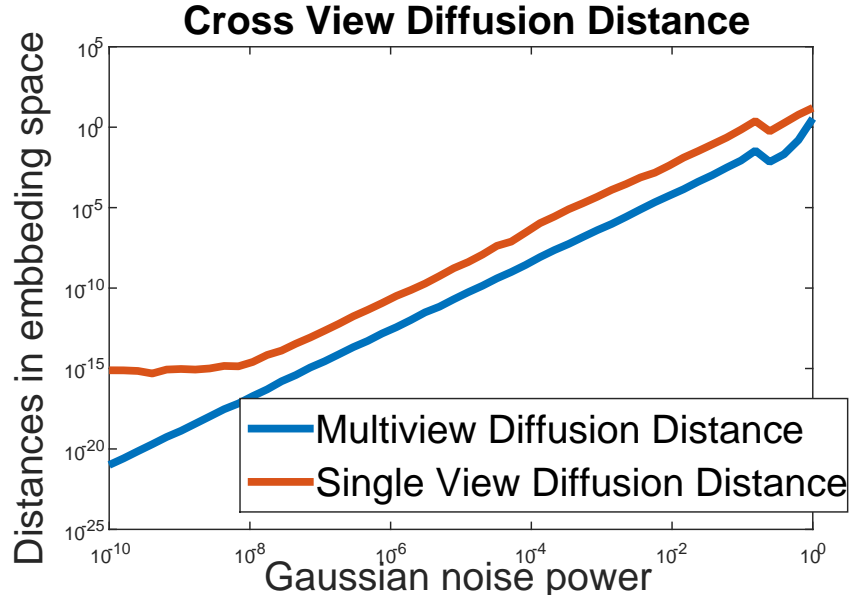


Fig. 9: Eigenvalues decay rate, comparison between the different mapping methods. Left figure mixture I, right figure mixture II.

$$\text{View II: } \mathbf{Y} = \begin{bmatrix} y_i^1 \\ y_i^2 \\ y_i^3 \end{bmatrix} = \begin{bmatrix} 4 \cos(0.9b_i) + 0.3 \cos(20b_i) \\ 4 \sin(0.9b_i) + 0.3 \sin(20b_i) \\ 0.1(6.3b_i - b_i^2) \end{bmatrix} \quad (28)$$

The 3-dimensional manifolds are presented in Fig. 10.

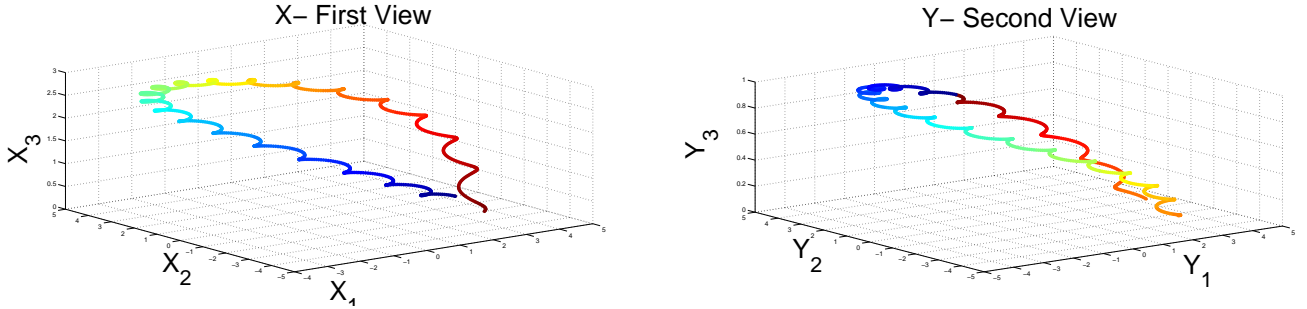


Fig. 10: Manifolds in both views. Both manifolds have some circular structure governed by the angle parameter a_i, b_i , colored by the points index.

The standard diffusion mapping (Kernel Product), has separated the manifold to a bow and a point as shown in Fig. 12. This structure does not represent any of the original structures, nor thus it reveal the underlying parameters (a_i, b_i) . On the other hand, our embedding captures the two structures, one for each view. As shown in Fig. 11, one structure represents the angle of a_i while the other represents the angle of b_i . The Euclidean distance in the new spaces preserves the mutual relations between points based on the geometrical relation in both views. Moreover both manifolds are in the same coordinate system, and this is a strong advantage as it enables to compare the manifolds in a lower dimensional space. The Euclidean distance in the new spaces preserves the mutual relations between points based on the geometrical structure of both views.

Helix B

We repeat the previous experiment with the following functions to generate datasets for View-I and View-II (X and Y respectively)

$$\text{View I: } \mathbf{X} = \begin{bmatrix} x_i^1 \\ x_i^2 \\ x_i^3 \end{bmatrix} = \begin{bmatrix} 4 \cos(5a_i) \\ 4 \sin(5a_i) \\ 4a_i \end{bmatrix} \quad (29)$$

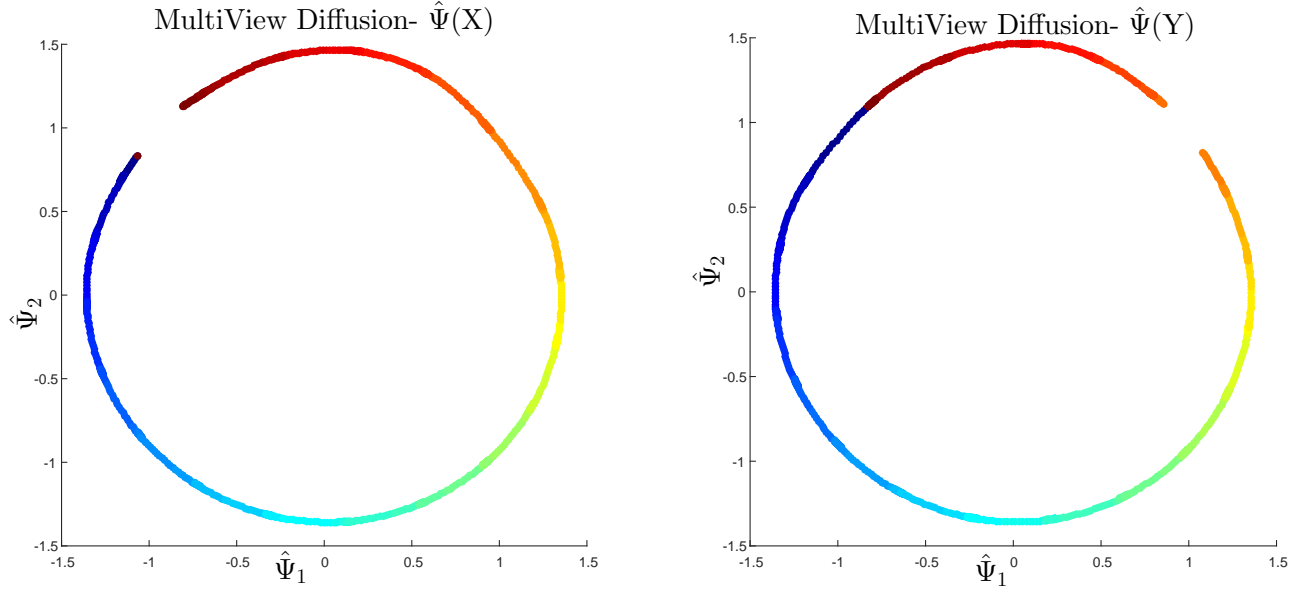


Fig. 11: The coupled mappings of the Helix computed using our proposed parametrization (Eqs. (13) and (14)).

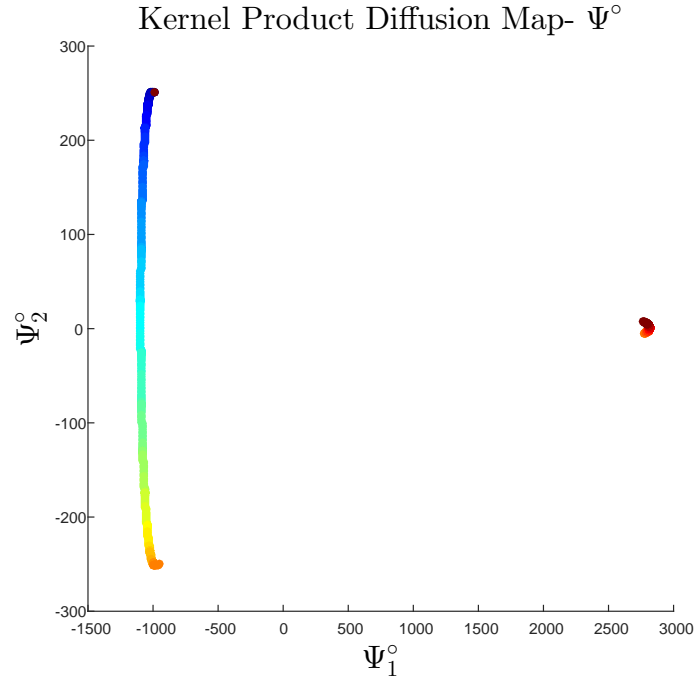


Fig. 12: A standard two dimensional diffusion mapping for the Helix, computed using the concatenation vector from both views (corresponding to kernel \mathbf{K}°).

$$\text{View II: } \mathbf{Y} = \begin{bmatrix} y_i^1 \\ y_i^2 \\ y_i^3 \end{bmatrix} = \begin{bmatrix} 4 \cos(5b_i) \\ 4 \sin(5b_i) \\ 4b_i \end{bmatrix} \quad (30)$$

Again we generate a 1000 points using $a_i \rightarrow [0, 2\pi]$, $b_i = a_i + 0.5\pi \bmod 2\pi$, where $i = 1, 2, 3, \dots, 1000$. The generated manifolds are presented in Fig. 13.

The extracted embeddings represent the governing parameters a_i, b_i , as can be viewed in Fig. 14. The kernel product embedding is presented in Fig. 15, the extracted embedding has again separated the point into two unconnected structures, and

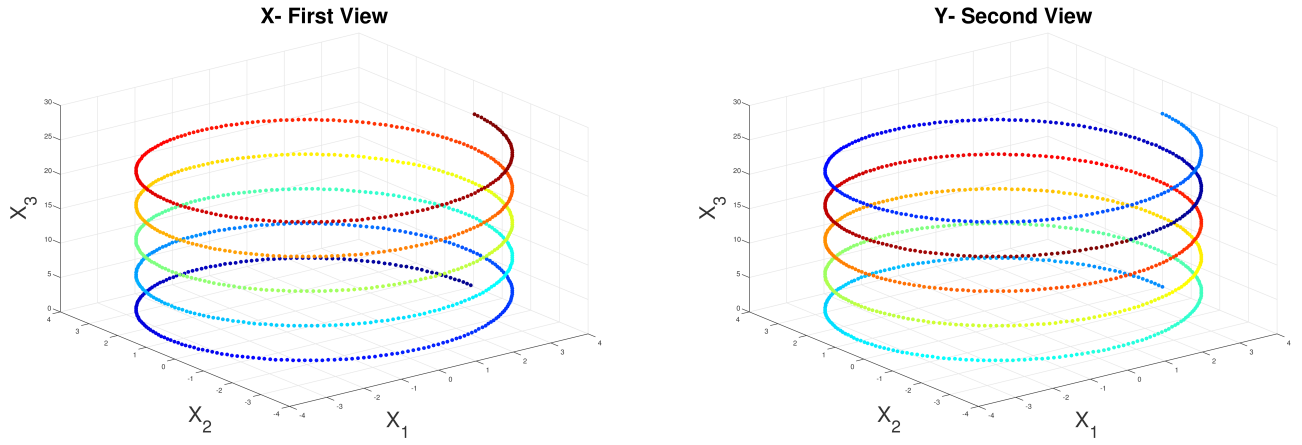


Fig. 13: Manifolds in both views. The angle is the governing parameter, each structure is “broken” between different data points.

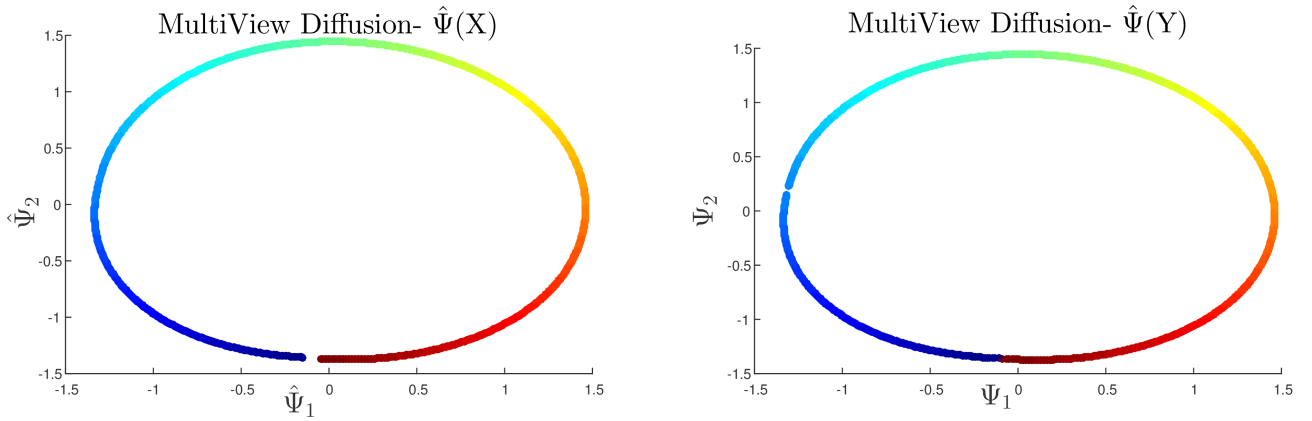


Fig. 14: The coupled mappings computed using our proposed parametrization (Eqs. 13 and 14).

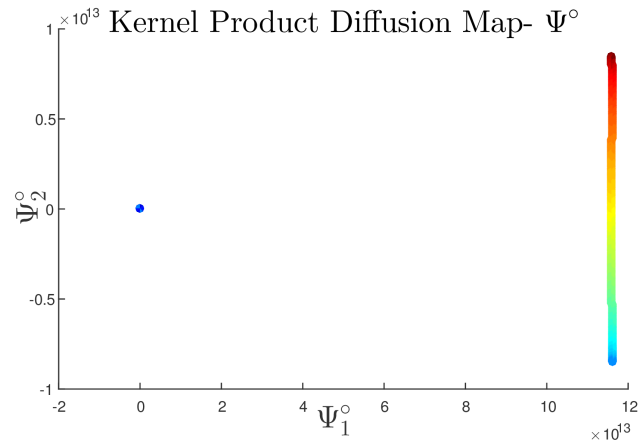


Fig. 15: A standard two dimensional diffusion mapping, computed using the concatenation vector from both views (corresponding to kernel K°).

does not represent the parameters well.

E. MultiView Video Sequence

Various examples have demonstrated the power of DM for extracting the underlying changing physical parameters from real datasets, such as images, audio, MRI [26], [7] and [27]. In this experiment we examine the proposed approach on a real life

dataset. We use two web cameras and a toy train, with a determined course. A sample frame from each view is presented in Fig. 16, the train's course has an "Eight" shaped structure. Extracting the underlying manifold from the set of images is interesting, as it allows to order the images according to the location along the track, and thus reveal the true underlying parameter of the processes.

The setting of the experiment is as follows, each camera records a set of images from a different angle. The resolution is (640X480) sampled at 30 frames per second. We collect $M = 220$ images from each view (camera), average the R,G,B values and down sample the resolution to (160X120), finally we reshape the matrix into a vector. The resulted set of vectors are denoted as \mathbf{X}, \mathbf{Y} , where $x_i, y_i \in R^{19200}$, ($1 \leq i \leq 220$). The order of the images is not of matter for the algorithm, in a normal setting one view is enough to extract the parameter governing the movement of the train along the course (and extract the natural order of the images). However, we use two distractions to create a scenario in which each view alone is insufficient for the extraction of the underlying parameter. The first distraction is a gap in the recording of each camera, we remove 20 consecutive frames from each of the view, at different time locations. Note that by doing this we have broken the bijective correspondence of some of the images in the sequence. However, even the approximate correspondence is sufficient for the manifold extraction. We apply standard DM on each view and extract a bow shaped manifold as can be viewed in Fig. 17. Applying DM on each view separately extracts the correct order of the points along the track, however the "missing" points have broken the circular structure of the expected manifold and created a bow shaped embedding. We use the Multiview to overcome the distraction, by applying the proposed framework and extracting two coupled mapping, the results are presented in Fig. 18. The proposed approach has overcome the distractions by smoothing the gap inherited in each view, using the connectivities from the "undistracted" view. Finally, we use the concatenation of both views and compute the Kernel Product Embedding, the results are presented in Fig. 19, again the structure of the manifold is distorted and incomplete due to the missing images.



Fig. 16: A sample image from both views (Left-View X, Right-View Y).

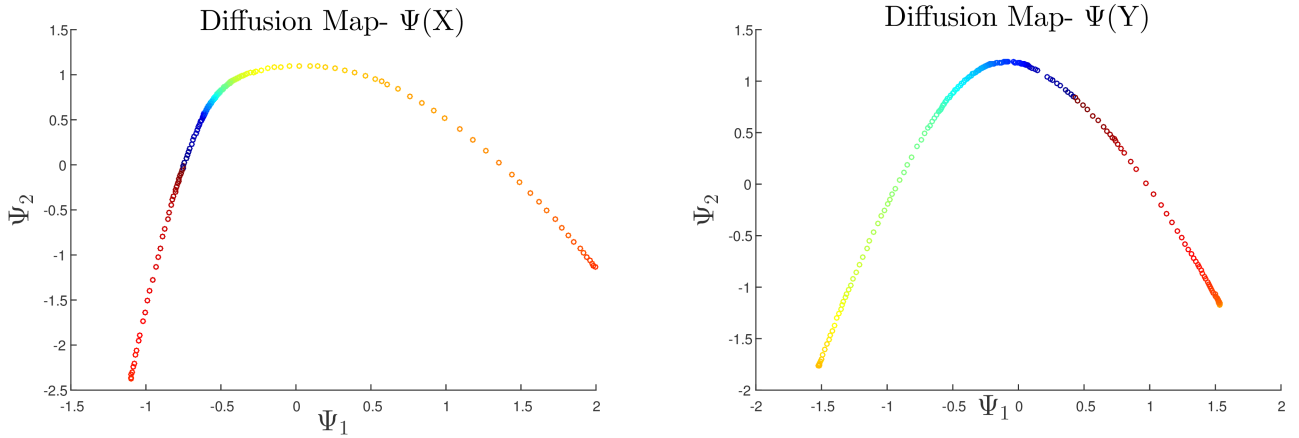


Fig. 17: The single view diffusion mappings (Left-Mapping $\Psi(\mathbf{X})$, Right-Mapping $\Psi(\mathbf{Y})$).

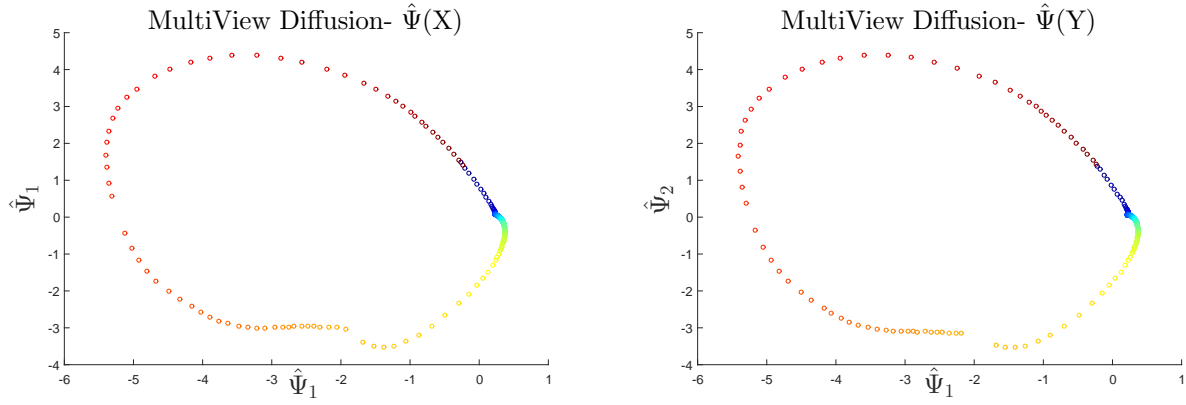


Fig. 18: The Multiview approach extracted embeddings (Left-Mapping $\hat{\Psi}(X)$, Right-Mapping $\hat{\Psi}(Y)$). Two gaps are visible, corresponding to the removed image sets

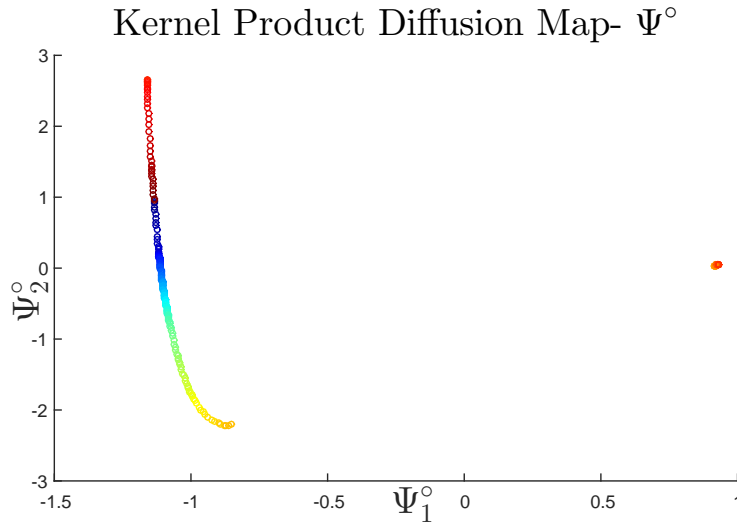


Fig. 19: A standard diffusion mapping (Kernel Product), computed using the concatenation vector from both views (corresponding to kernel K°).

We repeat the experiment this time inserting white Gaussian noise instead of 10 frames from each view, we compute the single view DM, the Kernel Product DM and the multiview DM. As presented in Fig. 20 the Gaussian noise has distorted the manifolds extracted in each view. The proposed approach has extracted two circular structures presented in Fig. 21, again the points are ordered according to the position along the track. This time the circular structure is unfolded, the gaps are visible in both embeddings. Applying the kernel product approach has extracted again a distorted manifold, this is presented in Fig. 22.

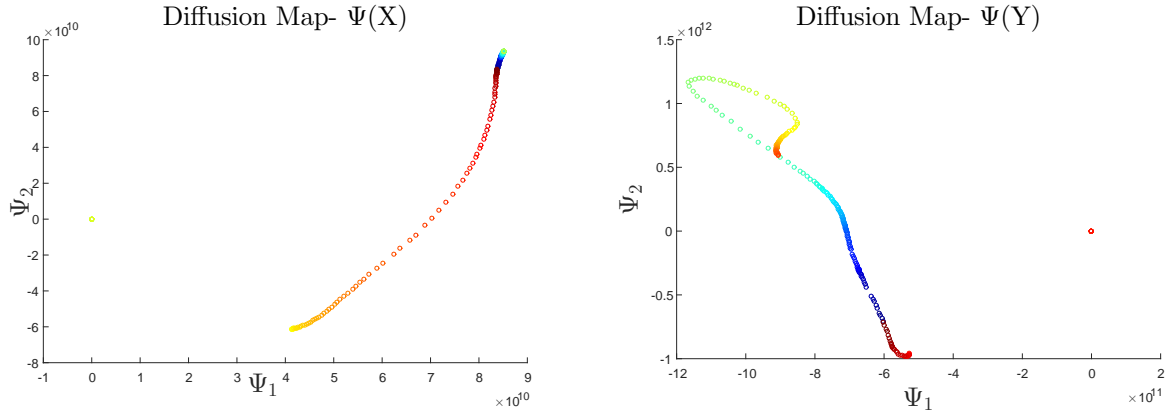


Fig. 20: A sample image from both views (Left-Mapping $\Psi(X)$, Right-Mapping $\Psi(Y)$).

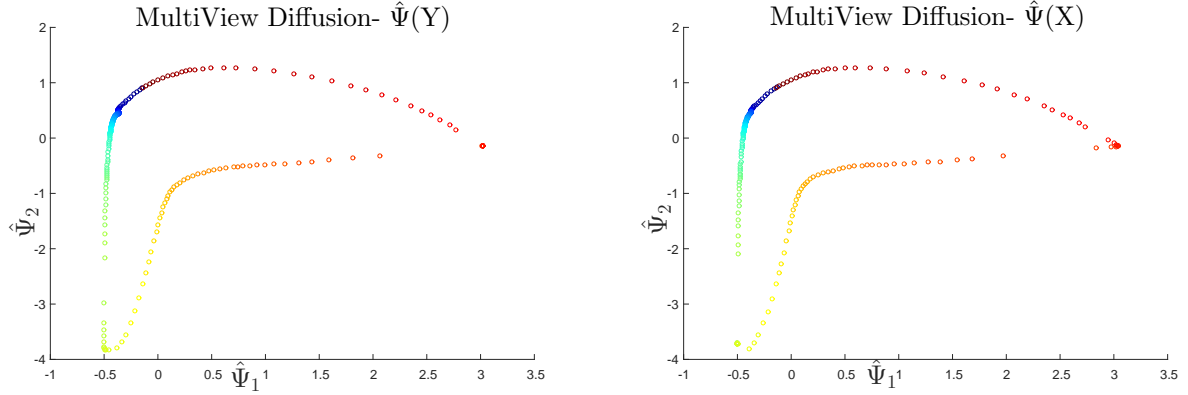


Fig. 21: The Multiview approach extracted embeddings (Left-Mapping $\hat{\Psi}(X)$, Right-Mapping $\hat{\Psi}(Y)$). Two gaps are visible, corresponding to the removed image sets

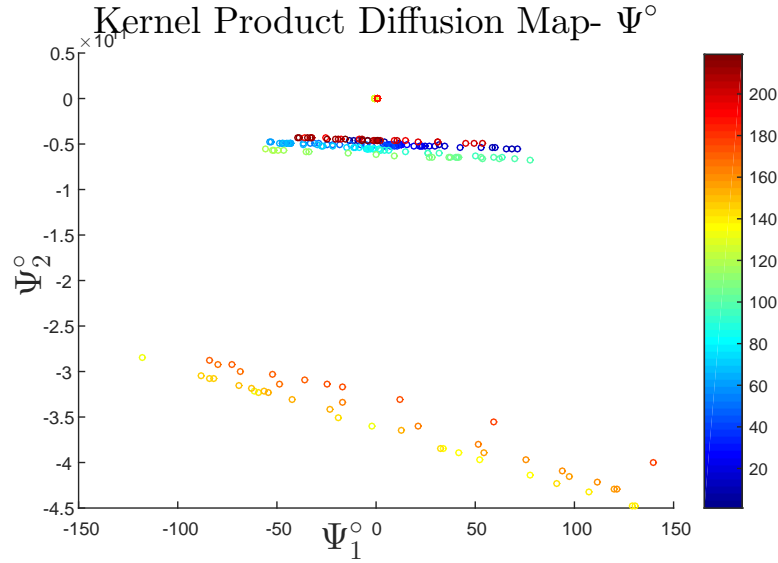


Fig. 22: A standard diffusion mapping (Kernel Product), computed using the concatenation vector from both views (corresponding to kernel K°).

VI. CONCLUSIONS

In this paper, we presented a framework for MultiView dimensionality reduction. The method enables to extract simultaneous embeddings from coupled embeddings. We enforce a cross domain probabilistic model, at a single time step the transition probabilities depend on the connectivities in both views. We have analyzed various theoretical aspects of the proposed method, and demonstrated the applicability on both artificial and real data sets. The experimental results have demonstrated the strength of the proposed framework when data is missing from each view, or each of the manifolds is deformed by some unknown function. The framework is applicable for various real life machine learning tasks, consisting of multiple views or modalities. We are considering the influence of various normalizations on the extracted embedding. Future work will include both application and theoretical analysis of such normalizations.

REFERENCES

- [1] I. Jolliffe, *Principal component analysis*, 2005, vol. 21.
- [2] J. B. Kruskal and W. M., "Multidimensional scaling," *Sage Publications. Beverly Hills*, 1977.
- [3] S. T. Roweis and L. K. Sau, "Nonlinear dimensionality reduction by local linear embedding," *Science*, vol. 290.5500, pp. 2323–2326, 2000.
- [4] W. Luo, "Face recognition based on laplacian eigenmaps," 2011, pp. 416 – 419.
- [5] R. R. Coifman and S. Lafon, "Diffusion maps," *Applied and Computational Harmonic Analysis*, vol. 21, pp. 5–30, 2006.
- [6] A. Singer and R. R. Coifman, "Non linear independent component analysis with diffusion maps," *Applied and Computational Harmonic Analysis*, vol. 25(2), pp. 226–239, 2008.
- [7] O. Lindenbaum, A. Yeredor, and I. Cohen, "Musical key extraction using diffusion maps," *Signal Processing*, 2015.
- [8] W. T. Freeman and J. B. Tenenbaum, "Learning bilinear models for two-factor problems in vision," in *Computer Vision and Pattern Recognition, Proceedings., IEEE Computer Society Conference on.* IEEE, 1997, pp. 554–560.
- [9] I. S. Helland, "Partial least squares regression and statistical models," *Scandinavian Journal of Statistics*, pp. 97–114, 1990.
- [10] K. Chaudhuri, S. M. Kakade, K. Livescu, and K. Sridharan, "Multi-view clustering via canonical correlation analysis," in *Proceedings of the 26th annual international conference on machine learning.* ACM, 2009, pp. 129–136.
- [11] A. Kumar, P. Rai, and H. Daume, "Co-regularized multi-view spectral clustering," in *Advances in Neural Information Processing Systems*, 2011, pp. 1413–1421.
- [12] D. Zhou and C. Burges, "Spectral clustering and transductive learning with multiple views," *Proceedings of the 24th international conference on Machine learning*, pp. 1159–1166, 2007.
- [13] B. Wang, J. Jiang, W. Wang, Z.-H. Zhou, and Z. Tu, "Unsupervised metric fusion by cross diffusion," in *Computer Vision and Pattern Recognition (CVPR), 2012 IEEE Conference on.* IEEE, 2012, pp. 2997–3004.
- [14] A. Kumar and H. Daumé, "A co-training approach for multi-view spectral clustering," in *Proceedings of the 28th International Conference on Machine Learning (ICML-11)*, 2011, pp. 393–400.
- [15] B. Boots and G. Gordon, "Two-manifold problems with applications to nonlinear system identification," 2012.
- [16] H. Hotelling, "Relations between two sets of variates," *Biometrika*, pp. 321–377, 1936.
- [17] V. R. de Sa, "Spectral clustering with two views," in *ICML workshop on learning with multiple views*, 2005.
- [18] S. Lafon, Y. Keller, and R. Coifman, "Data fusion and multicue data matching by diffusion maps," *IEEE Trans. Pattern Anal. Mach. Intell.*, vol. 28 no. 11, p. 17841797, 2006.
- [19] M. Hirn and R. Coifman, "Diffusion maps for changing data," *Applied and computational harmonic analysis*, 2013.
- [20] S. Yoel. Lector notes on spectral methods in data anlisys, <https://sites.google.com/site/yoelshkolnisky/teaching>.
- [21] S. Lafon, "Diffusion maps and geometric harmonics," *Ph.D dissertation Yale*, 2004.
- [22] T. Ando, "Majorization relations for hadamard products," *Linear Algebra and its Applications*, pp. 57–64, 1995.
- [23] G. Visick, "A weak majorization involving the matrices a , b and ab ," *Linear Algebra and its Applications*, vol. 224/224, pp. 731–744, 1995.
- [24] A. Y. Ng, M. I. Jordan, and Y. Weiss, "On spectral clustering1 analysis and an algorithm," *Proceedings of Advances in Neural Information Processing Systems. Cambridge, MA: MIT Press*, vol. 14, pp. 849–856, 2001.
- [25] M. Polito and P. Perona, "Grouping and dimensionality reduction by locally linear embedding," in *NIPS*, 2001, pp. 1255–1262.
- [26] S. Lafon, Y. Keller, and R. R. Coifman, "Data fusion and multicue data matching by diffusion maps," *Pattern Analysis and Machine Intelligence, IEEE Transactions on*, vol. 28, no. 11, pp. 1784–1797, 2006.
- [27] G. Piella, "Diffusion maps for multimodal registration," *Sensors*, vol. 14, no. 6, pp. 10 562–10 577, 2014.